# Matched transport of intense coupled beams in periodic solenoid focusing channels

C. Xiao* and L. Groening

*GSI Helmholtzzentrum für Schwerionenforschung GmbH, D-64291 Darmstadt, Germany*

(Received 14 November 2025; accepted 6 April 2026; published 27 May 2026)

Intense uncoupled beams are conventionally transported through periodic focusing lattices composed of linear optical elements that provide radial confinement against defocusing space-charge forces. In such systems, interplane coupling has traditionally been regarded as an undesirable perturbation. Recently, however, the concept of matched transport in periodic quadrupole focusing channels has been extended from uncoupled beams to those exhibiting significant correlations between the two transverse degrees of freedom [C. Xiao *et al.*, Periodic four-dimensional solution for transport of intense and coupled coasting beams through quadrupole channels, Phys. Rev. Accel. Beams **27**, 031602 (2024)]. Building on this development, the present work generalizes the full four-dimensional rms-moment matching formalism to periodic solenoid transport channels. A notable application of this approach, for instance, is the efficient transport of high-current, low-energy proton coasting beams.

DOI: 10.1103/rb9h-cz13

## I. INTRODUCTION

Low-energy beam transport systems for protons and heavy ions are most commonly realized using solenoids, whose axially symmetric magnetic fields provide effective transverse confinement. The dynamics of uncoupled beams in such systems, including the influence of space-charge effects, have been extensively investigated (see, for example, Ref. [1]). In contrast, the dynamics of coupled beams have received comparatively little attention, despite their equally important implications for accelerator design, optimization, and operation. Consequently, most existing beam transport lines and linear accelerator sections continue to be designed under the simplifying assumption of negligible transverse coupling.

For intense uncoupled beams, several matching methods have been established and successfully implemented in both design studies and operational practice. Classical approaches, which form the foundation of modern beam optics, are based on the coupled rms-envelope equations formulated by Sacherer [2,3]. These models assume a Kapchinskij-Vladimirskij (KV) distribution and evaluate linearized space-charge defocusing forces by representing the beam as a homogeneously charged, rms-equivalent ellipsoid. Within this framework, the rms-envelope equations remain self-consistent with the KV-type distribution, which constitutes an exact equilibrium solution of the linearized Vlasov equation.

Preservation of beam quality is a central objective in the transport of intense hadron beams. Traditionally, the quality of matching has been evaluated through the periodicity of the transverse beam envelopes, an approach sufficient in the absence of coupling between the horizontal and vertical phase planes. Although derived from the idealized KV distribution, rms-equivalent matching techniques have been successfully applied to realistic beams for several decades [4–6]. In practice, optimization of intense beam transport is typically accomplished by adjusting lattice parameters to accommodate prescribed emittances and intensities. Transverse confinement can be achieved using either quadrupole or solenoid focusing elements, and systematic comparisons of their performance are presented in Ref. [1]. Alternative approaches include tuning the phase advance along periodic structures [7], as well as accounting for coupling between the transverse and longitudinal phase planes [8].

The investigation presented here aims to establish a comprehensive four-dimensional (4D) matching framework for intense beams transported through periodic solenoid focusing channels. In this framework, 4D matching is defined as the extension of the periodicity condition from the transverse beam envelopes to all second-order beam moments, thereby ensuring complete covariance-matrix periodicity across successive lattice periods. This concept has previously been demonstrated for periodic quadrupole focusing channels [9], and its generalization to periodic solenoid focusing channels is developed in the present work.

*Contact author: c.xiao@gsi.de

The manuscript begins with a concise introduction to the problem of matched transport of intense beams in axially symmetric focusing lattices with significant transverse coupling, a topic introduced conceptually in [10]. It formalizes the fundamental concepts of projected rms emittance and eigenemittance as key metrics for quantifying beam quality and diagnosing interplane correlations in multidimensional phase space. Transfer matrices for two configurations of solenoid doublets are presented, establishing the linear symplectic framework for transport analysis, followed by a discussion of canonical variables in magnetic fields and their role in defining particle invariants and governing beam dynamics. Building upon this theoretical foundation, high-fidelity multiparticle tracking simulations are performed for intense coupled beams propagating through periodic solenoid channels with alternating polarity. These simulations examine the evolution of the 4D emittance, emphasizing growth mechanisms driven by nonlinear space-charge forces. A comparative analysis between full 4D rms-moment matching and conventional envelope matching demonstrates the superior effectiveness of the former in suppressing emittance growth and preserving intrinsic beam brightness under strongly coupled transport conditions.

## II. BASIC CONCEPT OF EMITTANCE

The transverse phase-space coordinates are described by a $4 \times 1$ column vector

$$\vec{r}(z) \coloneqq [\, x(z), x'(z), y(z), y'(z) \,]^{\mathrm{T}}, \tag{1}$$

where the prime denotes differentiation with respect to the longitudinal coordinate $z$. Accordingly, the angular divergences of the trajectory are defined as

$$x'(z) \coloneqq \frac{d[x(z)]}{dz}, \qquad y'(z) \coloneqq \frac{d[y(z)]}{dz}, \tag{2}$$

that is, as the derivatives of the transverse spatial coordinates $\mu$ (representing either $x$ or $y$) with respect to $z$. It is assumed that the transverse velocity components, given by $\beta c \mu'$, are small compared with the principal propagation velocity $\beta c$, where $c$ denotes the speed of light.

The linear transport of transverse phase-space coordinates from an initial to a final location can be expressed compactly as

$$[\vec{r}(z)]_{\mathrm{final}} = M \cdot [\vec{r}(z)]_{\mathrm{initial}}, \tag{3}$$

where the $4 \times 4$ transfer matrix $M$ is often represented in terms of $2 \times 2$ sub-blocks as

$$M \coloneqq \begin{bmatrix} M_{xx} & M_{xy} \\ M_{yx} & M_{yy} \end{bmatrix}. \tag{4}$$

A coupled beam is fully characterized by ten independent rms moments, conveniently arranged in a symmetric rms-moment beam matrix

$$\Sigma \coloneqq \begin{bmatrix} \Sigma_{xx} & \Sigma_{xy} \\ \Sigma_{xy}^{\mathrm{T}} & \Sigma_{yy} \end{bmatrix}, \tag{5}$$

where each $2 \times 2$ sub-block contains the rms moments associated with the corresponding phase planes.

Any linear transformation $M$ satisfying

$$J = M^{\mathrm{T}} \cdot J \cdot M, \qquad J \coloneqq \begin{bmatrix} 0 & 1 & 0 & 0 \\ -1 & 0 & 0 & 0 \\ 0 & 0 & 0 & 1 \\ 0 & 0 & -1 & 0 \end{bmatrix}, \tag{6}$$

is called symplectic. Under such a transformation, the beam matrix is transported from an initial to a final location according to

$$\Sigma_{\mathrm{final}} = M \cdot \Sigma_{\mathrm{initial}} \cdot M^{\mathrm{T}}. \tag{7}$$

The rms moments contained in the off-diagonal $2 \times 2$ submatrix, $\Sigma_{xy}$, quantify the strength of interplane coupling between the horizontal and vertical planes. A beam is considered coupled whenever at least one of these off-diagonal rms moments is nonzero.

The projected rms emittances are defined as the square roots of the determinants of the on-diagonal $2 \times 2$ submatrices of the beam rms-moment matrix

$$\varepsilon_x = \sqrt{\det(\Sigma_{xx})}, \qquad \varepsilon_y = \sqrt{\det(\Sigma_{yy})}, \tag{8}$$

and depend solely on the on-diagonal submatrices. They remain unaffected by the rms moments contained in the off-diagonal $2 \times 2$ submatrix $\Sigma_{xy}$.

In contrast, the transverse eigenemittances incorporate all interplane correlations and are defined as the positive invariants of the beam rms-moment matrix [11]

$$\varepsilon_{1,2} = \sqrt{-\frac{\mathrm{tr}[(\Sigma J)^2]}{4} \pm \sqrt{\frac{\mathrm{tr}^2[(\Sigma J)^2]}{16} - \det(\Sigma)}}, \tag{9}$$

where tr denotes the trace operator and the 4D emittance is defined as the square root of the determinant of the beam rms-moment matrix, i.e.,

$$\varepsilon_{4\mathrm{D}} = \sqrt{\det(\Sigma)} = \varepsilon_1 \varepsilon_2, \tag{10}$$

its value is equivalently given by the product of the transverse eigenemittances. Unlike the projected

emittances, which may vary in the presence of coupling, the 4D emittance remains strictly conserved under any linear symplectic transformation.

The projected rms emittances are preserved if and only if the transport matrix $M$ contains no coupling elements. In the special case where $M$ achieves complete decoupling of the beam, the resulting projected rms emittances coincide with the eigenemittances, corresponding to a completely decoupled beam. Consequently, eigenemittances, rather than projected rms emittances, provide the most fundamental characterization of transverse beam quality.

Dominant sources of transverse coupling originate from magnet misalignments, field imperfections, or unintended particle loss. For instance, if the upper-right portion of the beam is scraped off, the remaining beam acquires an interplane correlation, $\langle xy \rangle \neq 0$. In practice, the relatively weak coupling introduced by such effects can often be compensated with skew quadrupoles. However, complete suppression of coupling is generally unattainable, as higher-order magnets are routinely employed for lattice corrections, and the fringe fields of solenoids inherently generate additional correlations between the transverse planes. Consequently, even well-optimized transport systems retain a finite level of $x-y$ coupling. This inevitability has motivated the development of theoretical frameworks and matching methods based on eigenemittances, which serve as invariant measures of beam quality in the presence of interplane correlations. Moreover, coupling can also be deliberately introduced, for instance, to exploit the properties of circular beams or beams with angular momentum [12–15].

## III. BASIC CONCEPT OF TRANSPORTATION

Consider a relativistic particle beam with charge $q$ and longitudinal momentum $\gamma m\beta c$ propagating along the $z$ axis. All particles are assumed to share the same longitudinal velocity $\beta c$, which remains unaffected by variations in the longitudinal magnetic field $B_s$.

For analytical purposes, a solenoid can be conveniently modeled as consisting of three regions: an entrance fringe field, a uniform central field, and an exit fringe field.

In the entrance region, the radial kick imparted by the fringe field can be described using a thin-lens kick matrix within the hard-edge approximation

$$M_{\text{entry}} = \begin{bmatrix} 1 & 0 & 0 & 0 \\ 0 & 1 & \frac{\theta}{2D} & 0 \\ 0 & 0 & 1 & 0 \\ -\frac{\theta}{2D} & 0 & 0 & 1 \end{bmatrix}, \tag{11}$$

corresponding to the azimuthal ($\theta$) kick

$$x' \to x' + \frac{\theta}{2D} y, \qquad y' \to y' - \frac{\theta}{2D} x, \tag{12}$$

with

$$k \coloneqq \frac{\theta}{2D} = \frac{qB_s}{2\gamma m\beta c}, \tag{13}$$

where $D$ is the effective solenoid length. In this approximation, the entrance fringe field acts as a pure azimuthal kick, leaving the transverse positions $x$ and $y$ unchanged while altering the slopes $x'$ and $y'$.

Inside the uniform field region, the longitudinal magnetic field provides continuous transverse focusing while simultaneously coupling the horizontal and vertical phase planes through a rotation in 4D phase space. The corresponding transfer matrix is given by

$$M_{\text{body}} = \begin{bmatrix} 1 & \frac{D\sin(\theta)}{\theta} & 0 & \frac{D[1-\cos(\theta)]}{\theta} \\ 0 & \cos(\theta) & 0 & \sin(\theta) \\ 0 & -\frac{D[1-\cos(\theta)]}{\theta} & 1 & \frac{D\sin(\theta)}{\theta} \\ 0 & -\sin(\theta) & 0 & \cos(\theta) \end{bmatrix}. \tag{14}$$

In the exit region, the particle experiences a radial kick corresponding to the inverse of the entrance fringe matrix

$$M_{\text{exit}} = M_{\text{entry}}^{-1}. \tag{15}$$

Consequently, the transfer matrix of the solenoid is obtained by multiplying the entrance fringe, uniform field, and exit fringe matrices

$$\overrightarrow{M_{\text{sol}}} = M_{\text{exit}} \cdot M_{\text{body}} \cdot M_{\text{entry}}. \tag{16}$$

Employing the hard-edge approximation, the solenoid transfer map can also be decomposed into two fundamental components: an isotropic focusing term acting identically on both transverse planes and a Larmor rotation coupling the horizontal and vertical degrees of freedom.

Equivalently, the solenoid transfer map can be written as

$$\overrightarrow{M_{\text{sol}}} = \overrightarrow{M_{\text{rotation}}} \cdot M_{\text{focusing}} = M_{\text{focusing}} \cdot \overrightarrow{M_{\text{rotation}}}, \tag{17}$$

where the focusing transfer matrix

$$M_{\text{focusing}} = \begin{bmatrix} C & \frac{SD}{\Theta} & 0 & 0 \\ -\frac{S\Theta}{D} & C & 0 & 0 \\ 0 & 0 & C & \frac{SD}{\Theta} \\ 0 & 0 & -\frac{S\Theta}{D} & C \end{bmatrix}, \tag{18}$$

describes the motion of a simple harmonic oscillator in both horizontal and vertical planes, with a common phase advance $\Theta$, corresponding to equal linear focusing in the transverse directions.

The Larmor rotation transfer matrix

$$M^{\rightarrow}_{\text{rotation}} = \begin{bmatrix} C & 0 & S & 0 \\ 0 & C & 0 & S \\ -S & 0 & C & 0 \\ 0 & -S & 0 & C \end{bmatrix}, \tag{19}$$

simultaneously couples the transverse degrees of freedom through a rotation in 4D phase space.

Finally, the complete hard-edge solenoid transfer matrix is given by

$$M^{\rightarrow}_{\text{sol}} = \begin{bmatrix} C^2 & \frac{SCD}{\Theta} & SC & \frac{S^2D}{\Theta} \\ -\frac{SC\Theta}{D} & C^2 & -\frac{S^2\Theta}{D} & SC \\ -SC & -\frac{S^2D}{\Theta} & C^2 & \frac{SCD}{\Theta} \\ \frac{S^2\Theta}{D} & -SC & -\frac{SC\Theta}{D} & C^2 \end{bmatrix}, \tag{20}$$

with

$$C \coloneqq \cos(\Theta), \qquad S \coloneqq \sin(\Theta). \tag{21}$$

Reversing the longitudinal magnetic field modifies the transfer map only by changing the sign of the Larmor rotation, while the focusing term remains unchanged. The resulting transfer matrix reads

$$M^{\leftarrow}_{\text{sol}} = \begin{bmatrix} C^2 & \frac{SCD}{\Theta} & -SC & -\frac{S^2D}{\Theta} \\ -\frac{SC\Theta}{D} & C^2 & \frac{S^2\Theta}{D} & -SC \\ SC & \frac{S^2D}{\Theta} & C^2 & \frac{SCD}{\Theta} \\ -\frac{S^2\Theta}{D} & SC & -\frac{SC\Theta}{D} & C^2 \end{bmatrix}. \tag{22}$$

Here, $\Theta$ denotes the Larmor rotation angle of a single-particle trajectory as it traverses the solenoid, defined by

$$\Theta \coloneqq kD = \frac{qB_s}{2\gamma m\beta c}D. \tag{23}$$

The determinants of the on-diagonal $2 \times 2$ submatrices of $M^{\rightarrow}_{\text{sol}}$ and $M^{\leftarrow}_{\text{sol}}$ deviate from unity, indicating that the horizontal and vertical projected rms emittances are not conserved individually. Nevertheless, since both $M^{\rightarrow}_{\text{sol}}$ and $M^{\leftarrow}_{\text{sol}}$ are symplectic transformations, the eigenemittances remain strictly invariant, even though the projected rms emittances evolve due to solenoid-induced coupling.

A periodic solenoid doublet is modeled by inserting a drift space between two identical solenoids, as illustrated in Fig. 1. The resulting lattice cell consists of a repeating sequence of drift, solenoid, drift, solenoid, and drift. Two representative configurations of the solenoid doublet are examined to illustrate the characteristic transport behavior of coupled beams.

In the first configuration, the solenoids have equal polarities, which primarily increase the cumulative focusing strength while simultaneously enhancing the interplane coupling. In contrast, the second configuration employs solenoids with alternating polarities, which partially cancel the net rotational effect and thereby alter the balance between focusing and coupling.

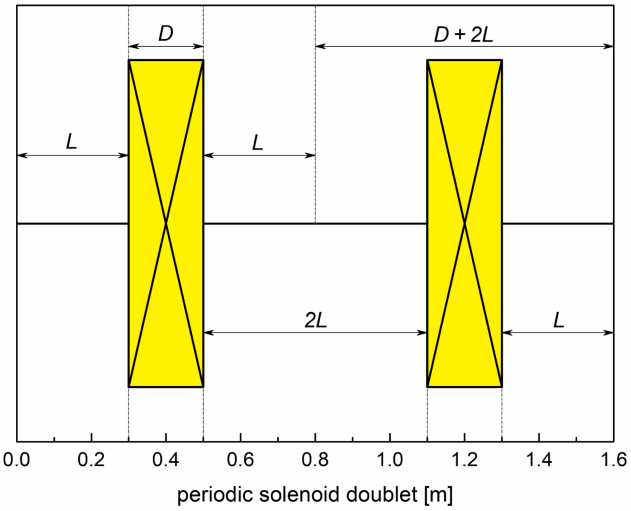


FIG. 1. Schematic of a periodic lattice consisting of two identical solenoids separated by drift spaces. The solenoid length is denoted by $D$, the separation between the solenoids is $2L$, and the length of one lattice period is therefore $2(D + 2L)$.

A lattice period is defined with its origin at the center of the intersolenoid drift. For a periodic solenoid doublet with alternating polarities, the zero-current transfer map can be expressed in the general block-symplectic form

$$\mathfrak{I} = \begin{bmatrix} \mathtt{A}_1 & \mathtt{A}_2 & \mathtt{A}_3 & \mathtt{A}_4 \\ \mathtt{B}_1 & \mathtt{B}_2 & \mathtt{B}_3 & \mathtt{B}_4 \\ \mathtt{C}_1 & \mathtt{C}_2 & \mathtt{C}_3 & \mathtt{C}_4 \\ \mathtt{D}_1 & \mathtt{D}_2 & \mathtt{D}_3 & \mathtt{D}_4 \end{bmatrix}, \tag{24}$$

and the input beam matrix at the entrance may contain up to ten independent rms moments

$$\Sigma_{\text{in}} = \begin{bmatrix} \mathtt{X}_1 & \mathtt{X}_2 & \mathtt{Z}_1 & \mathtt{Z}_2 \\ \cdots & \mathtt{X}_3 & \mathtt{Z}_3 & \mathtt{Z}_4 \\ \cdots & \cdots & \mathtt{Y}_1 & \mathtt{Y}_2 \\ \cdots & \cdots & \cdots & \mathtt{Y}_3 \end{bmatrix}. \tag{25}$$

A single half-period, extending from the entrance to the center of the solenoid doublet, consists of one solenoid lens symmetrically enclosed by two identical drift spaces. Accordingly, the transfer matrix for this half-period can be expressed as the ordered product of three matrices: a drift, the solenoid, and a second drift.

$$M^{\rightarrow}_{\frac{1}{2}\text{period}} = M_{\text{drift}} \cdot M^{\rightarrow}_{\text{sol}} \cdot M_{\text{drift}} = \begin{bmatrix} \Omega & \Psi \\ -\Psi & \Omega \end{bmatrix}, \tag{26}$$

with

$$\Omega \coloneqq C \cdot \begin{bmatrix} C - \frac{SL\Theta}{D} & L\left(2C - \frac{SL\Theta}{D} + \frac{SD}{L\Theta}\right) \\ -\frac{S\Theta}{D} & C - \frac{SL\Theta}{D} \end{bmatrix} = C \cdot \Gamma \quad (27)$$

and

$$\Psi \coloneqq S \cdot \begin{bmatrix} C - \frac{SL\Theta}{D} & L\left(2C - \frac{SL\Theta}{D} + \frac{SD}{L\Theta}\right) \\ -\frac{S\Theta}{D} & C - \frac{SL\Theta}{D} \end{bmatrix} = S \cdot \Gamma. \quad (28)$$

Thus, the transport matrix of a periodic solenoid doublet with equal polarities is given by the ordered product of the transfer matrices of its constituent half-periods.

$$\Im^{\oslash} = M^{\rightarrow}_{\frac{1}{2}\text{period}} \cdot M^{\rightarrow}_{\frac{1}{2}\text{period}} = \begin{bmatrix} \Omega^2 - \Psi^2 & 2\,\Omega\Psi \\ -2\,\Omega\Psi & \Omega^2 - \Psi^2 \end{bmatrix}, \quad (29)$$

where

$$\Omega^2 - \Psi^2 = (C^2 - S^2) \cdot \Gamma^2, \qquad 2\,\Omega\Psi = CS \cdot \Gamma^2, \quad (30)$$

and this lattice thus constitutes a fully coupled transport system.

If alternating polarities are adopted, the transport matrix for a single half-period takes the form

$$M^{\leftarrow}_{\frac{1}{2}\text{period}} = M_{\text{drift}} \cdot M^{\leftarrow}_{\text{sol}} \cdot M_{\text{drift}} = \begin{bmatrix} \Omega & -\Psi \\ \Psi & \Omega \end{bmatrix}, \quad (31)$$

and the overall transport matrix of the periodic solenoid doublet with alternating polarities reads

$$\Im^{\odot} = M^{\leftarrow}_{\frac{1}{2}\text{period}} \cdot M^{\rightarrow}_{\frac{1}{2}\text{period}} = \begin{bmatrix} \Omega^2 + \Psi^2 & 0 \\ 0 & \Omega^2 + \Psi^2 \end{bmatrix}, \quad (32)$$

with the off-diagonal sub-blocks vanishing, the lattice can be regarded as effectively decoupled, a behavior that has been previously demonstrated in [16].

The $2 \times 2$ submatrix $(\Omega^2 + \Psi^2)$ can be written as

$$\Omega^2 + \Psi^2 \coloneqq \begin{bmatrix} \left(C - \frac{SL\Theta}{D}\right)^2 - \frac{SL\Theta}{D}\left(2C - \frac{SL\Theta}{D} + \frac{SD}{L\Theta}\right) & 2L\left(C - \frac{SL\Theta}{D}\right)\left(2C - \frac{SL\Theta}{D} + \frac{SD}{L\Theta}\right) \\ -\frac{2SC\Theta}{D}\left(C - \frac{SL\Theta}{D}\right) & \left(C - \frac{SL\Theta}{D}\right)^2 - \frac{SL\Theta}{D}\left(2C - \frac{SL\Theta}{D} + \frac{SD}{L\Theta}\right) \end{bmatrix} = \Gamma^2 \quad (33)$$

noting that the on-diagonal elements of the 2×2 submatrix $(\Omega^2 + \Psi^2)$ are equal. In the subsequent sections, we focus on the solenoid doublet with alternating polarities, which corresponds to an effectively decoupled lattice.

## IV. CANONICAL VARIABLES IN SOLENOIDS

When a charged particle moves in a longitudinal magnetic field, its canonical conjugate variables are the transverse coordinates and canonical momenta, namely $(x, \tilde{p}_x)$ and $(y, \tilde{p}_y)$, where the canonical momenta are defined as

$$\tilde{p}_x = p_x + q \cdot A_x, \qquad \tilde{p}_y = p_y + q \cdot A_y, \quad (34)$$

with $A_x$ and $A_y$ denoting the transverse components of the vector potential. For a solenoid magnetic field, the vector potential has only an azimuthal component, which can be written as

$$A_\theta(r) = \frac{1}{2\pi r}\int_0^r B_z(z) 2\pi r^* dr^* = \frac{r}{2} \cdot B_z(z), \quad (35)$$

and the corresponding Cartesian components of the vector potential are

$$A_x = -\frac{y}{2} \cdot B_z(z), \qquad A_y = \frac{x}{2} \cdot B_z(z), \qquad A_z = 0. \quad (36)$$

From first principles, beam emittances must be defined in the phase planes of the canonical variables $(x, \tilde{p}_x)$ and $(y, \tilde{p}_y)$. In quadrupole focusing channels, these canonical variables coincide with the mechanical phase-space pairs $(x, p_x)$ and $(y, p_y)$. Consequently, in the presence of the longitudinal magnetic field, particle coordinates are most appropriately described in terms of the canonical variables rather than the mechanical momenta.

$$\tilde{x}' = x' - \nu \cdot y, \qquad \tilde{y}' = y' + \nu \cdot x, \quad (37)$$

where

$$\nu(z) = \frac{qB_z(z)}{2\gamma m\beta c}. \quad (38)$$

The corresponding rms moments in the canonical coordinates are then given by

$$\tilde{\mathtt{X}}_1 = \mathtt{X}_1, \quad \tilde{\mathtt{X}}_2 = \mathtt{X}_2 - \nu \cdot \mathtt{Z}_1, \quad \tilde{\mathtt{X}}_3 = \mathtt{X}_3 + \nu^2 \cdot \mathtt{Y}_1 - 2\nu \cdot \mathtt{Z}_3, \quad (39)$$

$$\tilde{\mathtt{Y}}_1 = \mathtt{Y}_1, \quad \tilde{\mathtt{Y}}_2 = \mathtt{Y}_2 + \nu \cdot \mathtt{Z}_1, \quad \tilde{\mathtt{Y}}_3 = \mathtt{Y}_3 + \nu^2 \cdot \mathtt{X}_1 + 2\nu \cdot \mathtt{Z}_2, \quad (40)$$

$$\tilde{\mathtt{Z}}_1 = \mathtt{Z}_1, \qquad \tilde{\mathtt{Z}}_2 = \mathtt{Z}_2 + \nu \cdot \mathtt{X}_1, \qquad \tilde{\mathtt{Z}}_3 = \mathtt{Z}_3 - \nu \cdot \mathtt{Y}_1, \quad (41)$$

$$\tilde{\mathtt{Z}}_4 = \mathtt{Z}_4 + \nu \cdot (\mathtt{X}_2 - \mathtt{Y}_2) - \nu^2 \cdot \mathtt{Z}_1. \quad (42)$$

Throughout this paper, $\tilde{\mathtt{Q}}$ denotes quantities evaluated using the modified rms moments: $\tilde{\mathtt{X}}_1, \tilde{\mathtt{X}}_2, \cdots, \tilde{\mathtt{Z}}_4$, whereas $\mathtt{Q}$ refers to the corresponding quantities computed from the conventional rms moments: $\mathtt{X}_1, \mathtt{X}_2, \cdots, \mathtt{Z}_4$. Unless explicitly stated otherwise, the modified form $\tilde{\mathtt{Q}}$ is employed throughout this paper. Outside the solenoids, where the longitudinal magnetic field vanishes, the two definitions coincide, i.e., $\tilde{\mathtt{Q}} = \mathtt{Q}$.

## V. BOUNDARIES FOR PERIODIC SOLUTIONS

This section addresses the boundary conditions for periodic solutions, which arise from the intrinsic properties of the lattice and the particle distribution. These conditions are independent of both the beam current and the specific form of the distribution, and thus apply equally to KV, Gaussian, or any other type of distribution. However, they do depend on the initial coupling configuration at the beginning of the lattice period. Three distinct coupling configurations are considered in detail: (i) A fully $x-y$ coupled particle distribution with negligible current, denoted by the matrix $\Sigma_{\mathrm{in}}^{\odot}$. (ii) A fully $x-y$ decoupled particle distribution with significant space charge, denoted by the matrix $\Sigma_{\mathrm{in}}^{\oplus}$. (iii) A partially $x-y$ coupled particle distribution, in which only the components $\mathtt{Z}_1$ and $\mathtt{Z}_4$ are nonzero, with significant space charge, denoted by the matrix $\Sigma_{\mathrm{in}}^{\otimes}$.

It should be emphasized that the three sets of eigenemittances associated with the matrices $\Sigma_{\mathrm{in}}^{\odot}$, $\Sigma_{\mathrm{in}}^{\oplus}$, and $\Sigma_{\mathrm{in}}^{\otimes}$ are the same. In a well-matched periodic transport channel, the Twiss parameters repeat from period to period, and this periodicity condition serves as a cornerstone for both the analytical treatment and numerical optimization of the focusing lattice. Establishing such periodic solutions is particularly important in the presence of solenoid focusing and space-charge forces.

### A. Fully coupled beam with zero current ($\Sigma_{\mathrm{in}}^{\odot}$)

For any matched beam, the transverse envelopes reach their maximum at the center of each solenoid and their minimum at the center of each drift space. Consequently, the beam waists are located at the entrance of a periodic solenoid doublet with alternating polarities, where the rms moments satisfy

$$\mathtt{X}_2 = \frac{\mathtt{X}_1'}{2} = 0, \qquad \mathtt{Y}_2 = \frac{\mathtt{Y}_1'}{2} = 0, \tag{43}$$

thus, we consider a coupled asymmetric input beam represented by

$$\Sigma_{\mathrm{in}}^{\odot} = \begin{bmatrix} \mathtt{X}_1 & 0 & \mathtt{Z}_1 & \mathtt{Z}_2 \\ \cdots & \mathtt{X}_3 & \mathtt{Z}_3 & \mathtt{Z}_4 \\ \cdots & \cdots & \mathtt{Y}_1 & 0 \\ \cdots & \cdots & \cdots & \mathtt{Y}_3 \end{bmatrix}, \tag{44}$$

where all off-diagonal elements can be nonzero.

According to Eqs. (32) and (33), the corresponding zero-current transfer matrix of the solenoid doublet is

$$\Im^{\odot} = \begin{bmatrix} \mathtt{A}_1 & \mathtt{A}_2 & 0 & 0 \\ \mathtt{B}_1 & \mathtt{A}_1 & 0 & 0 \\ 0 & 0 & \mathtt{A}_1 & \mathtt{A}_2 \\ 0 & 0 & \mathtt{B}_1 & \mathtt{A}_1 \end{bmatrix}, \tag{45}$$

and behind the solenoid doublet, the matched uncoupled rms moments satisfy

$$\begin{aligned} \mathtt{X}_1 &= \mathtt{A}_1^2 \cdot \mathtt{X}_1 + \mathtt{A}_2^2 \cdot \mathtt{X}_3 \\ \mathtt{X}_2 &= \mathtt{A}_1\mathtt{B}_1 \cdot \mathtt{X}_1 + \mathtt{A}_1\mathtt{A}_2 \cdot \mathtt{X}_3 = 0 \\ \mathtt{X}_3 &= \mathtt{B}_1^2 \cdot \mathtt{X}_1 + \mathtt{A}_1^2 \cdot \mathtt{X}_3 \\ \mathtt{Y}_1 &= \mathtt{A}_1^2 \cdot \mathtt{Y}_1 + \mathtt{A}_2^2 \cdot \mathtt{Y}_3 \\ \mathtt{Y}_2 &= \mathtt{A}_1\mathtt{B}_1 \cdot \mathtt{Y}_1 + \mathtt{A}_1\mathtt{A}_2 \cdot \mathtt{Y}_3 = 0 \\ \mathtt{Y}_3 &= \mathtt{B}_1^2 \cdot \mathtt{Y}_1 + \mathtt{A}_1^2 \cdot \mathtt{Y}_3 \end{aligned} \tag{46}$$

similarly, the interplane rms moments satisfy

$$\begin{aligned} \mathtt{Z}_1 &= \mathtt{A}_1^2 \cdot \mathtt{Z}_1 + \mathtt{A}_1\mathtt{A}_2 \cdot \mathtt{Z}_2 + \mathtt{A}_1\mathtt{A}_2 \cdot \mathtt{Z}_3 + \mathtt{A}_2^2 \cdot \mathtt{Z}_4 \\ \mathtt{Z}_2 &= \mathtt{A}_1\mathtt{B}_1 \cdot \mathtt{Z}_1 + \mathtt{A}_1^2 \cdot \mathtt{Z}_2 + \mathtt{A}_2\mathtt{B}_1 \cdot \mathtt{Z}_3 + \mathtt{A}_1\mathtt{A}_2 \cdot \mathtt{Z}_4 \\ \mathtt{Z}_3 &= \mathtt{A}_1\mathtt{B}_1 \cdot \mathtt{Z}_1 + \mathtt{A}_2\mathtt{B}_1 \cdot \mathtt{Z}_2 + \mathtt{A}_1^2 \cdot \mathtt{Z}_3 + \mathtt{A}_1\mathtt{A}_2 \cdot \mathtt{Z}_4 \\ \mathtt{Z}_4 &= \mathtt{B}_1^2 \cdot \mathtt{Z}_1 + \mathtt{A}_1\mathtt{B}_1 \cdot \mathtt{Z}_2 + \mathtt{A}_1\mathtt{B}_1 \cdot \mathtt{Z}_3 + \mathtt{A}_1^2 \cdot \mathtt{Z}_4 \end{aligned} \tag{47}$$

imposing the symplectic condition $\det(\Im^{\odot}) = 1$ leads to

$$\mathtt{A}_1^2 - \mathtt{A}_2\mathtt{B}_1 = 1, \tag{48}$$

and the following relations

$$\frac{\mathtt{X}_1}{\mathtt{X}_3} = \frac{\mathtt{Y}_1}{\mathtt{Y}_3} = \frac{\mathtt{Z}_1}{\mathtt{Z}_4} = -\frac{\mathtt{A}_2}{\mathtt{B}_1}, \qquad \frac{\mathtt{Z}_2}{\mathtt{Z}_3} = -1, \tag{49}$$

must be satisfied.

It should be emphasized that the parameters: $\mathtt{A}_1$, $\mathtt{A}_2$, and $\mathtt{B}_1$ of the $2 \times 2$ submatrix $(\Omega^2 + \Psi^2)$ are determined solely by the lattice configuration and are completely independent of the initial particle distribution.

For a solenoid doublet with equal polarities, the corresponding transfer matrix can be written as

$$\mathfrak{I}^{\oslash} = \mathfrak{I}^{\odot} \cdot \vec{M}_{\text{rotation}} \cdot \vec{M}_{\text{rotation}}, \tag{50}$$

by exploiting the commutativity of rotation and drift matrices, as well as that of focusing and rotation matrices, the matched solution satisfies

$$\frac{\mathtt{X}_1}{\mathtt{X}_3} = \frac{\mathtt{Y}_1}{\mathtt{Y}_3} = -\frac{\mathtt{A}_2}{\mathtt{B}_1}, \qquad \mathtt{Z}_1 = \mathtt{Z}_4 = 0, \qquad \frac{\mathtt{X}_1}{\mathtt{Y}_1} = -\frac{\mathtt{Z}_2}{\mathtt{Z}_3} = 1. \tag{51}$$

Consequently, an equal-polarity solenoid doublet can transport only upright beams periodically, i.e., beams for which the coupled rms moment $\mathtt{Z}_1$ vanishes. In contrast, an alternating-polarity solenoid doublet can also support the periodic transport of nonupright beams, characterized by a nonzero coupled rms moment, $\mathtt{Z}_1 \neq 0$.

### B. Fully decoupled beam with high current ($\boldsymbol{\Sigma}_{\text{in}}^{\oplus}$)

Next, we consider an uncoupled asymmetric beam at the entrance of the alternating-polarity solenoid doublet, defined by

$$\boldsymbol{\Sigma}_{\text{in}}^{\oplus} = \begin{bmatrix} \mathtt{X}_1 & 0 & 0 & 0 \\ \cdots & \mathtt{X}_3 & 0 & 0 \\ \cdots & \cdots & \mathtt{Y}_1 & 0 \\ \cdots & \cdots & \cdots & \mathtt{Y}_3 \end{bmatrix}, \tag{52}$$

and the corresponding transport matrix, including linear space-charge forces, is assumed to take the block-diagonal form

$$\mathfrak{I}_{\text{sc}}^{\oplus} = \begin{bmatrix} \mathtt{A}_1 & \mathtt{A}_2 & 0 & 0 \\ \mathtt{B}_1 & \mathtt{A}_1 & 0 & 0 \\ 0 & 0 & \mathtt{C}_3 & \mathtt{C}_4 \\ 0 & 0 & \mathtt{D}_3 & \mathtt{C}_3 \end{bmatrix}, \tag{53}$$

In the absence of interplane coupling, the matched uncoupled rms moments behind the solenoid doublet satisfy

$$\begin{aligned} \mathtt{X}_1 &= \mathtt{A}_1^2 \cdot \mathtt{X}_1 + \mathtt{A}_2^2 \cdot \mathtt{X}_3 \\ \mathtt{X}_2 &= \mathtt{A}_1\mathtt{B}_1 \cdot \mathtt{X}_1 + \mathtt{A}_1\mathtt{A}_2 \cdot \mathtt{X}_3 = 0 \\ \mathtt{X}_3 &= \mathtt{B}_1^2 \cdot \mathtt{X}_1 + \mathtt{A}_1^2 \cdot \mathtt{X}_3 \\ \mathtt{Y}_1 &= \mathtt{C}_3^2 \cdot \mathtt{Y}_1 + \mathtt{C}_4^2 \cdot \mathtt{Y}_3 \\ \mathtt{Y}_2 &= \mathtt{C}_3\mathtt{D}_3 \cdot \mathtt{Y}_1 + \mathtt{C}_3\mathtt{C}_4 \cdot \mathtt{Y}_3 = 0 \\ \mathtt{Y}_3 &= \mathtt{D}_3^2 \cdot \mathtt{Y}_1 + \mathtt{C}_3^2 \cdot \mathtt{Y}_3 \end{aligned} \tag{54}$$

and by imposing the symplectic condition $\det(\mathfrak{I}_{\text{sc}}^{\oplus}) = 1$ once again, we obtain

$$\mathtt{A}_1^2 - \mathtt{A}_2\mathtt{B}_1 = 1, \qquad \mathtt{C}_3^2 - \mathtt{C}_4\mathtt{D}_3 = 1. \tag{55}$$

Consequently, the matched beam aspect ratios in the horizontal and vertical phase planes are expressed as

$$\frac{\mathtt{X}_1}{\mathtt{X}_3} = \frac{\mathtt{A}_2^2}{1-\mathtt{A}_1^2} = \frac{1-\mathtt{A}_1^2}{\mathtt{B}_1^2} = -\frac{\mathtt{A}_2}{\mathtt{B}_1} \tag{56}$$

and

$$\frac{\mathtt{Y}_1}{\mathtt{Y}_3} = \frac{\mathtt{C}_4^2}{1-\mathtt{C}_3^2} = \frac{1-\mathtt{C}_3^2}{\mathtt{D}_3^2} = -\frac{\mathtt{C}_4}{\mathtt{D}_3}, \tag{57}$$

reflecting the focusing characteristics of the solenoid doublet in each transverse plane.

It should be noted that the parameters: $\mathtt{A}_1, \mathtt{A}_2, \cdots, \mathtt{D}_4$ of the beam matrix, $\mathfrak{I}_{\text{sc}}^{\oplus}$, are no longer determined exclusively by the external lattice configuration. In the presence of space-charge forces, these parameters depend explicitly on both the beam current and the particle distribution. Consequently, unlike the negligible-current case where they are purely lattice-determined, the transport is governed by the self-consistent interplay between external lattice focusing and internal space-charge defocusing.

### C. Partially coupled beam with high current ($\boldsymbol{\Sigma}_{\text{in}}^{\otimes}$)

The following analysis assumes that the matching section can provide an asymmetric beam with vanishing coupled rms moments: $\mathtt{Z}_2 = \mathtt{Z}_3 = 0$, at the entrance of the solenoid doublet. The corresponding input beam matrix is then given by

$$\boldsymbol{\Sigma}_{\text{in}}^{\otimes} = \begin{bmatrix} \mathtt{X}_1 & 0 & \mathtt{Z}_1 & 0 \\ \cdots & \mathtt{X}_3 & 0 & \mathtt{Z}_4 \\ \cdots & \cdots & \mathtt{Y}_1 & 0 \\ \cdots & \cdots & \cdots & \mathtt{Y}_3 \end{bmatrix}, \tag{58}$$

and the corresponding transfer matrix is then given by

$$\mathfrak{I}_{\text{sc}}^{\otimes} = \begin{bmatrix} \mathtt{A}_1 & \mathtt{A}_2 & \mathtt{A}_3 & \mathtt{A}_4 \\ \mathtt{B}_1 & \mathtt{A}_1 & \mathtt{B}_3 & \mathtt{B}_4 \\ \mathtt{C}_1 & \mathtt{C}_2 & \mathtt{C}_3 & \mathtt{C}_4 \\ \mathtt{D}_1 & \mathtt{D}_2 & \mathtt{D}_3 & \mathtt{C}_3 \end{bmatrix}. \tag{59}$$

The space-charge contribution to the transport matrix, $\mathfrak{I}_{\text{sc}}^{\otimes}$, is determined by the spatial components of the beam matrix $\boldsymbol{\Sigma}_{\text{in}}^{\otimes}$. In particular, it depends explicitly on the rms moments: $\mathtt{X}_1$, $\mathtt{Y}_1$, and $\mathtt{Z}_1$, which define the size and orientation of the rms-ellipse in the transverse $x$–$y$ plane. Consequently, the matched rms moments downstream of this alternating-polarity solenoid doublet are given by

$$\begin{aligned}
X_1 &= A_1^2 \cdot X_1 + A_2^2 \cdot X_3 + A_3^2 \cdot Y_1 + A_4^2 \cdot Y_3 + 2A_1A_3 \cdot Z_1 + 2A_2A_4 \cdot Z_4 \\
X_2 &= A_1B_1 \cdot X_1 + A_1A_2 \cdot X_3 + A_3B_3 \cdot Y_1 + A_4B_4 \cdot Y_3 + (A_1B_3 + A_3B_1) \cdot Z_1 + (A_2B_4 + A_1A_4) \cdot Z_4 = 0 \\
X_3 &= B_1^2 \cdot X_1 + A_1^2 \cdot X_3 + B_3^2 \cdot Y_1 + B_4^2 \cdot Y_3 + 2B_1B_3 \cdot Z_1 + 2A_1B_4 \cdot Z_4 \\
Y_1 &= C_1^2 \cdot X_1 + C_2^2 \cdot X_3 + C_3^2 \cdot Y_1 + C_4^2 \cdot Y_3 + 2C_1C_3 \cdot Z_1 + 2C_2C_4 \cdot Z_4 \\
Y_2 &= C_1D_1 \cdot X_1 + C_2D_2 \cdot X_3 + C_3D_3 \cdot Y_1 + C_4C_3 \cdot Y_3 + (C_1D_3 + C_3D_1) \cdot Z_1 + (C_2C_3 + C_4D_2) \cdot Z_4 = 0 \\
Y_3 &= D_1^2 \cdot X_1 + D_2^2 \cdot X_3 + D_3^2 \cdot Y_1 + C_3^2 \cdot Y_3 + 2D_1D_3 \cdot Z_1 + 2D_2C_3 \cdot Z_4
\end{aligned} \tag{60}$$

and

$$\begin{aligned}
Z_1 &= A_1C_1 \cdot X_1 + A_2C_2 \cdot X_3 + A_3C_3 \cdot Y_1 + A_4C_4 \cdot Y_3 + (A_1C_3 + A_3C_1) \cdot Z_1 + (A_2C_4 + A_4C_2) \cdot Z_4 \\
Z_2 &= A_1D_1 \cdot X_1 + A_2D_2 \cdot X_3 + A_3D_3 \cdot Y_1 + A_4C_3 \cdot Y_3 + (A_1D_3 + A_3D_1) \cdot Z_1 + (A_2C_3 + A_4D_2) \cdot Z_4 = 0 \\
Z_3 &= B_1C_1 \cdot X_1 + A_1C_2 \cdot X_3 + B_3C_3 \cdot Y_1 + B_4C_4 \cdot Y_3 + (B_1C_3 + B_3C_1) \cdot Z_1 + (A_1C_4 + B_4C_2) \cdot Z_4 = 0 \\
Z_4 &= B_1D_1 \cdot X_1 + A_1D_2 \cdot X_3 + B_3D_3 \cdot Y_1 + B_4D_4 \cdot Y_3 + (B_1D_3 + B_3D_1) \cdot Z_1 + (A_1D_4 + B_4D_2) \cdot Z_4
\end{aligned} \tag{61}$$

based on these relations, a dedicated numerical routine implemented in Mathcad [17] is employed to iteratively adjust the 16 matrix elements: $m_1, m_2, \cdots, m_{16}$, so as to reproduce the prescribed rms moments: $X_1, X_2, \cdots, Z_4$, at the entrance of the solenoid doublet.

A comprehensive derivation of the elements of the input beam matrix $\Sigma_{in}$ and of the space-charge-modified cell transfer matrix $\mathfrak{I}_{sc}$ is presented in [9]. However, this derivation should be repeated here in the Appendix A. In the analytical calculation, each solenoid and drift section is subdivided into sufficiently small slices. The beam is propagated through each slice using the linear transport matrix, and the space-charge kick is applied at the end of each slice. By repeating this procedure along the lattice, the self-consistent space-charge forces associated with the tilted beam are accurately represented, while the 4D symplectic structure of the transport is preserved.

A systematic iterative procedure has been developed and implemented in the Mathcad program to obtain a self-consistent periodic solution for the high-current coupled beam by starting from the zero-current periodic solution and alternately propagating the beam through a single lattice period at finite beam current, thereby computing the space-charge-modified transport matrix and updating the matching parameters to enforce periodicity.

## VI. NUMERICAL METHODOLOGY

At the starting position, a coasting proton beam with a kinetic energy of 150 keV and a current of 10 mA is considered. Its initial state is characterized by an uncoupled second-moment beam matrix, $\Sigma$, with transverse eigenemittances of 24.25 and 212.5 mm mrad. Each solenoid has an effective length of $D = 20$ cm, and the drift space between adjacent solenoids is $L = 30$ cm, resulting in a total lattice period of $2(D + 2L) = 160$ cm. The nominal axial magnetic field in each solenoid is set to 0.30 T.

### A. Fully coupled beam with zero current ($\Sigma_{in}^{\odot}$)

The artificial matching section is modeled by a symplectic transport matrix, satisfying

$$\Sigma_{in}^{\odot} = \Re(\aleph) \cdot \Sigma \cdot \Re^{T}(\aleph). \tag{62}$$

To determine the periodic solution for the input beam matrix $\Sigma_{in}^{\odot}$, the detailed structure of the matching section is not required. Nevertheless, it is represented by a general $4 \times 4$ transfer matrix comprising 16 elements

$$\Re(\aleph) = \Re(m_1, m_2, \cdots, m_{16}) = \begin{bmatrix} m_1 & m_2 & m_3 & m_4 \\ m_5 & m_6 & m_7 & m_8 \\ m_9 & m_{10} & m_{11} & m_{12} \\ m_{13} & m_{14} & m_{15} & m_{16} \end{bmatrix}. \tag{63}$$

Although initially unknown, the 16 elements of $\Re$ must satisfy the symplectic condition of Eq. (6). The output beam matrix $\Sigma_{out}^{\odot}$ at the exit of the solenoid doublet is then expressed as

$$\Sigma_{out}^{\odot} = \mathfrak{I}^{\odot} \cdot \Sigma_{in}^{\odot} \cdot (\mathfrak{I}^{\odot})^{T} = (\mathfrak{I}^{\odot} \cdot \Re) \cdot \Sigma \cdot (\mathfrak{I}^{\odot} \cdot \Re)^{T}. \tag{64}$$

Consequently, the input beam matrix, $\Sigma_{in}^{\odot}$, and the initial beam matrix, $\Sigma$, must share identical pairs of eigenemittances; however, their projected rms emittances may differ due to the coupling introduced by the solenoids.

Based on the analytical results presented in Sec. V A, a coupled asymmetric input beam matrix, $\Sigma_{in}^{\odot}$, has been numerically obtained at the entrance of the solenoid doublet with alternating polarities. Expressed in units of mm and mrad, it reads

$$\Sigma_{\mathrm{in}}^{\odot} = \begin{bmatrix} +53.13 & 0 & -39.31 & +62.17 \\ \cdots & +124.7 & -62.17 & -92.27 \\ \cdots & \cdots & +101.4 & 0 \\ \cdots & \cdots & \cdots & +238.0 \end{bmatrix}, \quad (65)$$

which is identical to the output beam matrix $\Sigma_{\mathrm{out}}^{\odot}$ at the exit of the solenoid doublet, i.e.,

$$\Sigma_{\mathrm{out}}^{\odot} = \begin{bmatrix} +53.13 & 0 & -39.31 & +62.17 \\ \cdots & +124.7 & -62.17 & -92.27 \\ \cdots & \cdots & +101.4 & 0 \\ \cdots & \cdots & \cdots & +238.0 \end{bmatrix}. \quad (66)$$

The corresponding effective transport matrix without space charge, expressed in units of m and rad, is

$$\Im^{\odot} = \begin{bmatrix} -0.597 & +0.524 & 0 & 0 \\ -1.230 & -0.597 & 0 & 0 \\ 0 & 0 & -0.597 & +0.524 \\ 0 & 0 & -1.230 & -0.597 \end{bmatrix}. \quad (67)$$

The transport matrix, $\Im^{\odot}$, is block-diagonal, featuring identical $2 \times 2$ submatrices along the diagonal for both transverse planes. The input beam matrix, $\Sigma_{\mathrm{in}}^{\odot}$, and the transport matrix, $\Im^{\odot}$, jointly satisfy Eqs. (43) and (49). The corresponding phase advances, obtained from $\Im^{\odot}$, are equal in both planes $\sigma_x = \sigma_y = 126.6°$.

### B. Fully decoupled beam with high current ($\Sigma_{\mathrm{in}}^{\oplus}$)

The linear space-charge forces arising from the electric self-fields can be calculated analytically, as demonstrated by Sacherer for uncoupled beams with a KV distribution, where the phase-space ellipses are upright and uniformly populated. In the coupled case, these self-forces are first evaluated in the tilted laboratory frame, then projected onto the upright frame before being incorporated into the beam dynamics. A detailed description of this procedure is provided in [9].

A beamline composed of multiple solenoids, transporting an intense coupled coasting proton beam, can be modeled as a sequence of symplectic transport matrices. In this approach, both solenoids and drift spaces are subdivided into short slices. Transport through each short slice is performed using the corresponding symplectic transfer map without space-charge effects, followed by the application of a space-charge kick.

Considering an uncoupled asymmetric beam matrix, a solution at the entrance of the periodic solenoid doublet has been obtained using a dedicated numerical routine implemented in Mathcad. Expressed in units of mm and mrad, the matrix reads

$$\Sigma_{\mathrm{in}}^{\oplus} = \begin{bmatrix} +19.79 & +0.009 & +0.003 & +0.010 \\ \cdots & +29.70 & +0.031 & -0.715 \\ \cdots & \cdots & +149.6 & +0.068 \\ \cdots & \cdots & \cdots & +301.7 \end{bmatrix}, \quad (68)$$

and the corresponding effective transport matrix, which accounts for linearized space-charge forces, is expressed in units of m and rad as

$$\Im_{\mathrm{sc}}^{\oplus} = \begin{bmatrix} -0.206 & +0.799 & -0.000 & +0.002 \\ -1.199 & -0.205 & +0.003 & +0.001 \\ +0.001 & +0.002 & -0.466 & +0.623 \\ +0.003 & +0.000 & -1.257 & -0.465 \end{bmatrix}, \quad (69)$$

and the corresponding phase advances are calculated as $\sigma_x^{\mathrm{sc}} = 101.9°$ and $\sigma_y^{\mathrm{sc}} = 117.7°$. Compared with the zero-current case, the reduction in phase advances clearly illustrates the depressing effect of space charge on beam focusing.

Finally, the output beam matrix behind the solenoid doublet, expressed in units of mm and mrad, is

$$\Sigma_{\mathrm{out}}^{\oplus} = \begin{bmatrix} +19.79 & +0.009 & +0.008 & -0.008 \\ \cdots & +29.70 & +0.041 & -0.729 \\ \cdots & \cdots & +149.6 & +0.068 \\ \cdots & \cdots & \cdots & +301.7 \end{bmatrix}, \quad (70)$$

and is practically identical to the input beam matrix $\Sigma_{\mathrm{in}}^{\oplus}$.

Equations (43), (56), and (57) are well satisfied by the beam matrix $\Sigma_{\mathrm{in}}^{\oplus}$ and the transport matrix $\Im_{\mathrm{sc}}^{\oplus}$. Notably, the diagonal submatrices of $\Im_{\mathrm{sc}}^{\oplus}$ are not identical, revealing a residual asymmetry between the horizontal and vertical planes.

### C. Partially coupled beam with high current ($\Sigma_{\mathrm{in}}^{\otimes}$)

The matching section can also generate a coupled beam at the entrance of the periodic solenoid doublet, obtained from the full 4D periodic solution calculated using an alternative numerical routine implemented in Mathcad. The resulting input matched beam matrix, expressed in units of mm and mrad, is given by

$$\Sigma_{\mathrm{in}}^{\otimes} = \begin{bmatrix} +82.54 & +0.058 & +64.89 & +0.020 \\ \cdots & +160.4 & +0.041 & +135.9 \\ \cdots & \cdots & +86.89 & +0.019 \\ \cdots & \cdots & \cdots & +171.0 \end{bmatrix}, \quad (71)$$

and the corresponding effective transport matrix (in units of m and rad) reads

$$\Im_{\mathrm{sc}}^{\otimes} = \begin{bmatrix} -0.331 & +0.715 & -0.130 & -0.088 \\ -1.224 & -0.330 & -0.029 & -0.130 \\ -0.130 & -0.088 & -0.340 & +0.706 \\ -0.029 & -0.130 & -1.232 & -0.340 \end{bmatrix}, \quad (72)$$

and the corresponding space-charge-modified phase advances are computed as $\sigma_x^{\mathrm{sc}} = 109.3°$ and $\sigma_y^{\mathrm{sc}} = 109.9°$.

The output beam matrix behind the solenoid doublet, expressed in units of mm and mrad, is given by

$$\Sigma_{\mathrm{out}}^{\otimes} = \begin{bmatrix} +82.55 & +0.054 & +64.89 & +0.005 \\ \cdots & +160.4 & +0.055 & +135.9 \\ \cdots & \cdots & +86.89 & +0.023 \\ \cdots & \cdots & \cdots & +171.0 \end{bmatrix}. \quad (73)$$

It is again observed that the output beam matrix is effectively identical to the input beam matrix $\Sigma_{\mathrm{in}}^{\otimes}$. The system of Eqs. (60) and (61) is accurately satisfied by the beam matrix $\Sigma_{\mathrm{in}}^{\otimes}$ and the transport matrix $\mathfrak{I}_{\mathrm{sc}}^{\otimes}$, confirming the periodicity, stability, and self-consistency of the matched intense coupled beam.

The computed numerical values of the transfer matrices $\mathfrak{I}^{\odot}$, $\mathfrak{I}_{\mathrm{sc}}^{\oplus}$, and $\mathfrak{I}_{\mathrm{sc}}^{\otimes}$ exhibit substantial differences, with no apparent convergence among them. These discrepancies result from the linearized space-charge forces, which modify the effective focusing strengths and thus alter the transport coefficients.

## VII. PARTICLE TRACKING SIMULATIONS

This section presents a detailed particle tracking analysis of partially coupled beams, represented by the beam matrix $\Sigma_{\mathrm{in}}^{\otimes}$, in the presence of nonlinear space-charge defocusing forces. The first subsection focuses on the accurate modeling of solenoid magnetic fringe fields, while the subsequent subsections present the results of the particle tracking simulations.

### A. Modeling of solenoid magnetic fields

The transport matrix of a hard-edge solenoid provides an exact description within the framework of linear optics. However, real solenoids exhibit fringe fields at both the entrance and exit, which can influence transverse coupling and the evolution of beam emittances. For accurate particle tracking simulations, these fringe fields must be modeled in a manner that preserves the effective on-axis field strength $B_s$ and the effective length $D$ of the corresponding hard-edge approximation.

Within a sufficiently small radius, the axial and radial magnetic field components can be expressed in terms of the on-axis field using the paraxial approximation

$$B_z(r,z) = B_z(z), \qquad B_r(r,z) = -\frac{r}{2}\cdot\frac{\partial B_z(z)}{\partial z}. \quad (74)$$

Figure 2 depicts the longitudinal magnetic field profiles employed in the periodic solenoid doublet.

In the simplified hard-edge approximation, the longitudinal field is assumed to be perfectly uniform, dropping abruptly at the entrance and exit. Although this idealization

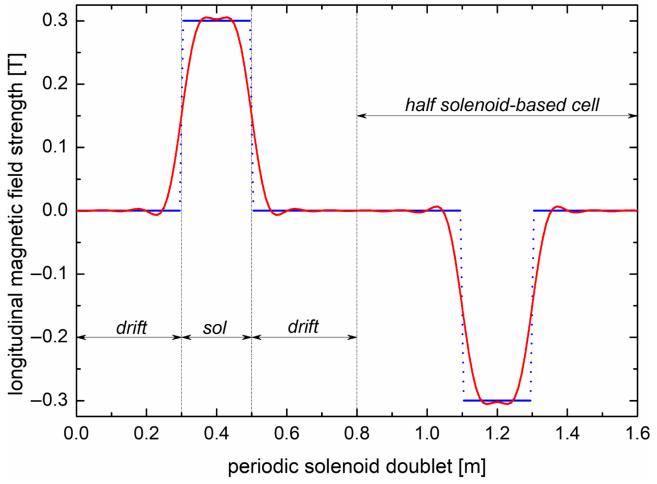


FIG. 2. On-axis (longitudinal) magnetic field profiles through a periodic solenoid doublet with alternating polarities. Blue markers indicate the hard-edge model, while red markers represent the soft-edge model, smoothed using the `FFTFilter` low-pass technique in Origin.

is mathematically convenient and often adequate for introductory analytical studies, it neglects the physical presence of fringe fields. In practice, a solenoid is more accurately represented by the soft-edge model, in which the longitudinal field transitions gradually at both the entrance and exit, rather than changing instantaneously.

Accurate modeling of fringe fields is particularly important in long solenoid channels, where even small discrepancies in the local focusing strength can accumulate over many lattice periods, resulting in significant deviations in beam dynamics. Incorporating soft-edge effects modifies the effective focusing strength of each solenoid, thereby influencing the phase advance, the evolution of the beam envelope, and the preservation of 4D emittance.

Integrating a soft-edge longitudinal magnetic field profile over the first half-period yields the corresponding effective field strength

$$\frac{1}{D}\int_0^{D+2L} B_z(z)\,\mathrm{d}z \approx B_s = 0.3011. \quad (75)$$

In general, in the presence of fringe fields in a soft-edge solenoid reduces the effective focusing strength compared with that of an ideal hard-edge solenoid having the same nominal field strength.

### B. Particle dynamics in periodic solenoid doublets

In this subsection, single-particle tracking simulations are performed using both hard-edge and soft-edge models of periodic solenoid doublets. The initial spatial distribution of particles, shown in Fig. 3, serves as the starting point for this comparison.

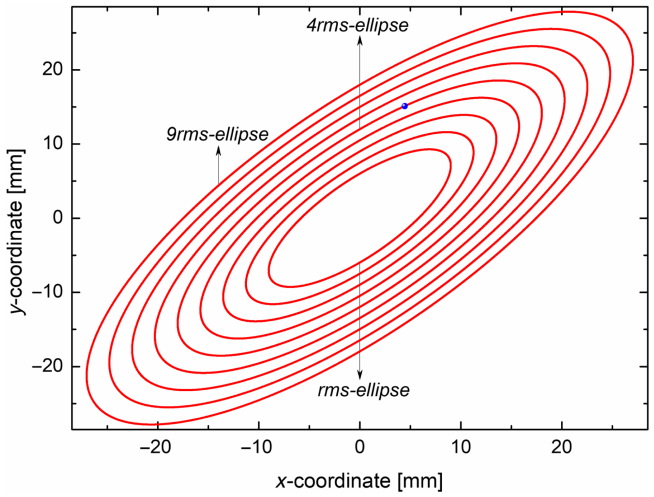


FIG. 3. Spatial distribution at the entrance of a solenoid doublet, derived from the beam matrix $\Sigma_{\mathrm{in}}^{\otimes}$. Red dots indicate the initial particle positions and the reference particle is shown in blue.

The sizes and orientations of the concentric ellipses are determined by the spatial components of the matrix $\Sigma_{\mathrm{in}}^{\otimes}$, specifically $\mathtt{X}_1$, $\mathtt{Y}_1$, and $\mathtt{Z}_1$. The solenoid is aligned along the $z$ axis, with each particle considered off axis, and its magnetic field is assumed to consist solely of longitudinal and radial components.

Consequently, the cross product of the particle velocity along $z$ with the radial position vector $(z, r)$ generates a force in the azimuthal $(\theta)$ direction, which does not contribute to net focusing. As a result, the beam experiences only a rotation around the $z$ axis. In contrast, if the particle has a velocity component in the $\theta$ direction, the cross product of $(z, \theta)$ with $(z, r)$ produces a radially directed focusing force.

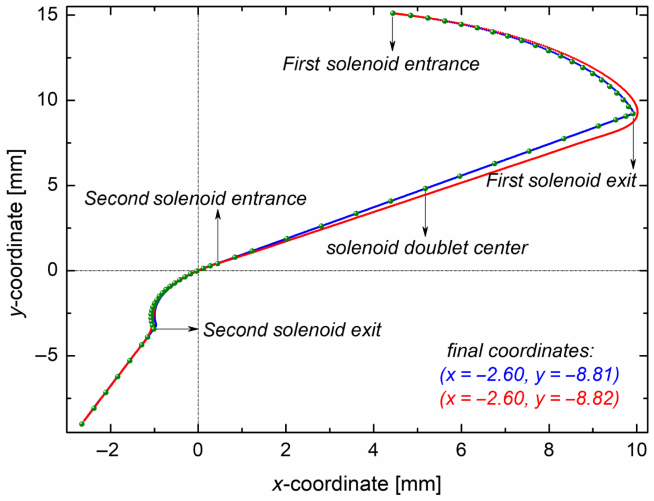


FIG. 4. Trajectory evolution of the reference particle through a solenoid doublet for the hard-edge model (blue) and the soft-edge model (red) together with analytical predictions from the transfer matrix formalism (olive).

In the single-particle tracking simulation, the reference particle is propagated through the solenoid doublet to its exit. To ensure identical exit positions and momenta in both models, the longitudinal magnetic field is scaled by a factor of 1.000 in the hard-edge model and 1.066 in the soft-edge model. The resulting single-particle trajectories from both models are presented in Fig. 4. The results for the reference particle show excellent agreement between the trajectories predicted by the hard-edge and soft-edge models.

In the multiparticle tracking simulation, the entrance distribution is propagated through the solenoid doublet, and the resulting exit distributions are shown in Fig. 5. Particles initialized within a smaller ellipse (corresponding to the 1× rms-ellipse) approximately preserve their elliptical shape after transport through both the hard-edge and soft-edge longitudinal magnetic fields, confirming the validity of the linear optics approximation in this regime. In contrast, particles launched on a larger ellipse (corresponding to the 9× rms-ellipse) exhibit pronounced nonlinear distortions, reflecting the increasing influence of fringe fields at larger amplitudes.

### C. Particle dynamics in periodic solenoid channels

Although idealized, the KV-type distribution provides a useful benchmark for simulations and serves as an rms-equivalent reference for studying matching conditions. In practice, however, space-charge forces are inherently nonlinear, and these nonlinearities can significantly influence beam dynamics. Consequently, realistic beams are more accurately represented by a Gaussian-type distribution.

Multiparticle tracking simulations are performed using the particle-in-cell code Beampath [18]. The coasting proton beam is represented by a Gaussian distribution of 30,000 macroparticles, rms-equivalent to the matrix $\Sigma_{\mathrm{in}}^{\otimes}$.

Figure 6 shows the evolution of the 2× rms-beam sizes through the periodic solenoid focusing channel, modeled using soft-edge solenoids. If 4D rms-moment matching is applied, the beam envelopes in both the horizontal and vertical planes exhibit strict periodicity.

In a solenoid field, the eigenemittances remain invariant and are conserved in rms-moment tracking, provided that only linearized space-charge forces are considered. In contrast, multiparticle tracking inherently accounts for the full nonlinear dynamics of space-charge effects. Multiparticle tracking simulations through the periodic solenoid focusing channel, initialized with the periodic solution defined by $\Sigma_{\mathrm{in}}^{\otimes}$, reveal noticeable emittance growth. The square root of the 4D emittance increases by 17% for the hard-edge model, compared with 10% for the soft-edge model. These results indicate that, although nonlinear space-charge forces contribute to emittance growth in both cases, the hard-edge approximation systematically overestimates the effect.

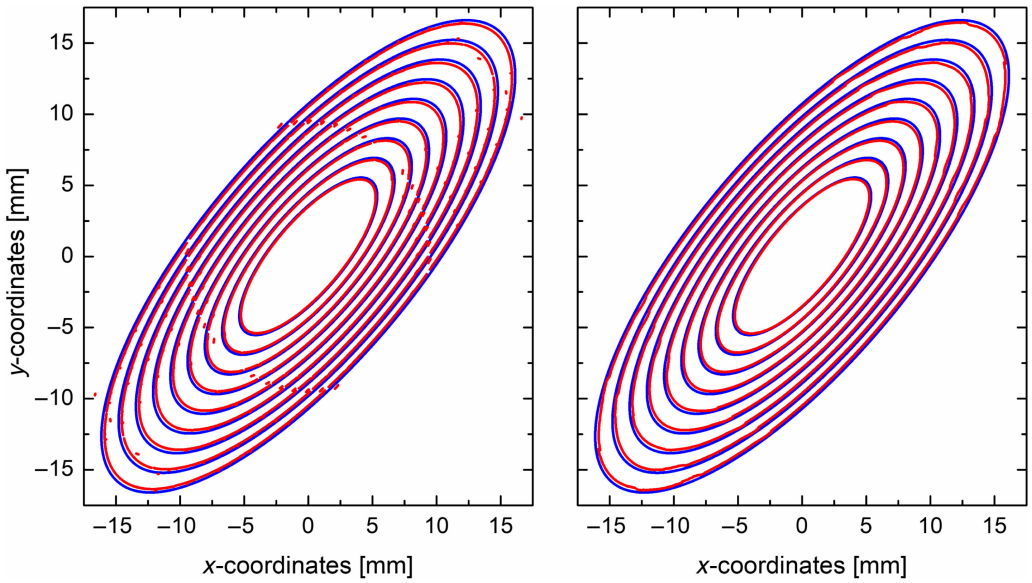


FIG. 5. Spatial distributions at the exit of the periodic solenoid doublet obtained from analytical calculations (left and right, blue) and from multiparticle tracking simulations using the hard-edge (left, red) and soft-edge (right, red) models, respectively. The hard-edge model exhibits minor anomalies, with a small fraction of particles showing slight positional deviations, whereas the soft-edge model closely agrees with the analytical prediction.

To illustrate the effects of mismatch, the 2× rms-beam sizes are shown in Figs. 7 and 8 for a 20% variation in solenoid field strength relative to the nominal value, while the initial particle distribution remains unchanged.

If the initial particle distribution, rms-equivalent to the matrix $\Sigma_{\text{in}}^{\otimes}$, is injected into the solenoid focusing channel with the field strength that is either reduced or increased, it no longer corresponds to the matched solution: (i) Under-focusing: occurs when the focusing strength is insufficient, causing the beam envelope to expand beyond its nominal size. (ii) Over-focusing: occurs when the focusing strength is excessive, leading the beam envelope to contract or oscillate more strongly than expected.

Complementary to the results shown in Figs. 6–8, Fig. 9 presents the six 2D projections of the phase-space ellipses corresponding to the particle distribution at the entrance, characterized by the beam matrix $\Sigma_{\text{in}}^{\otimes}$, and at the exit of the first lattice period.

Figure 10 illustrates the dependence of the corresponding square roots of the 4D emittances at the exit of the

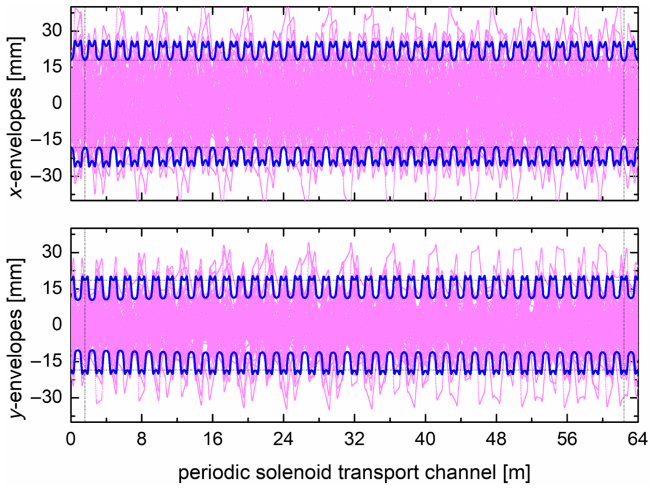


FIG. 6. Transverse 2× rms-beam sizes and representative particle trajectories for an intense, coupled coasting proton beam. The initial Gaussian distribution is rms-equivalent to the matrix $\Sigma_{\text{in}}^{\otimes}$, and each solenoid is modeled using the soft-edge approximation at the nominal field strength of 0.30 T. The periodic solenoid focusing channel consists of 40 periods.

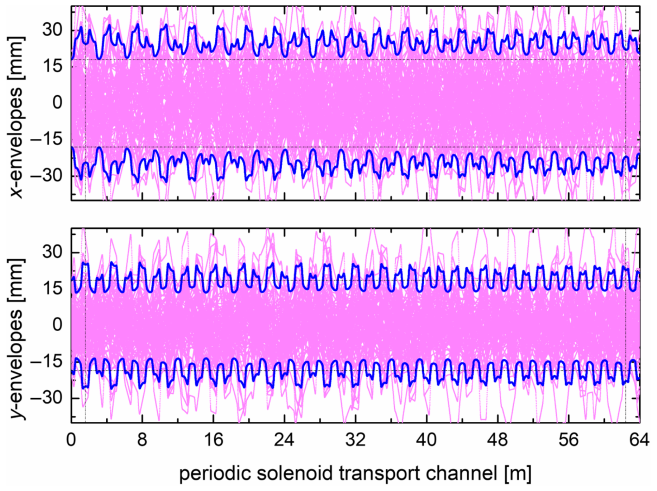


FIG. 7. Configuration is identical to that shown in Fig. 6, except that the solenoid field is reduced to 0.24 T, representing a 20% decrease relative to the nominal value.

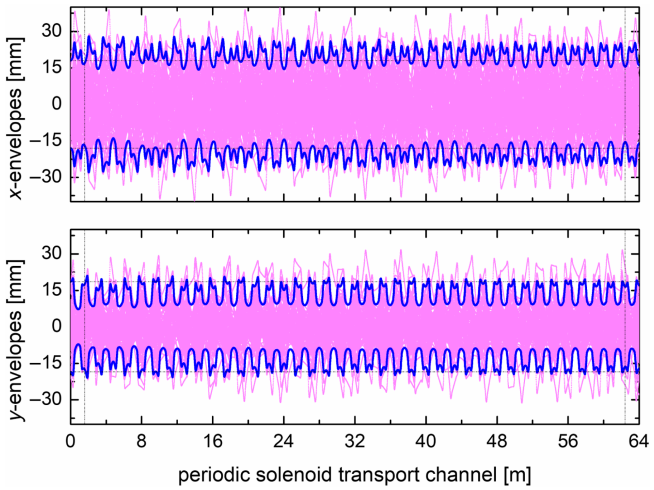


FIG. 8. Configuration is identical to that shown in Fig. 6, except that the solenoid field is increased to 0.36 T, corresponding to a 20% enhancement relative to the nominal value.

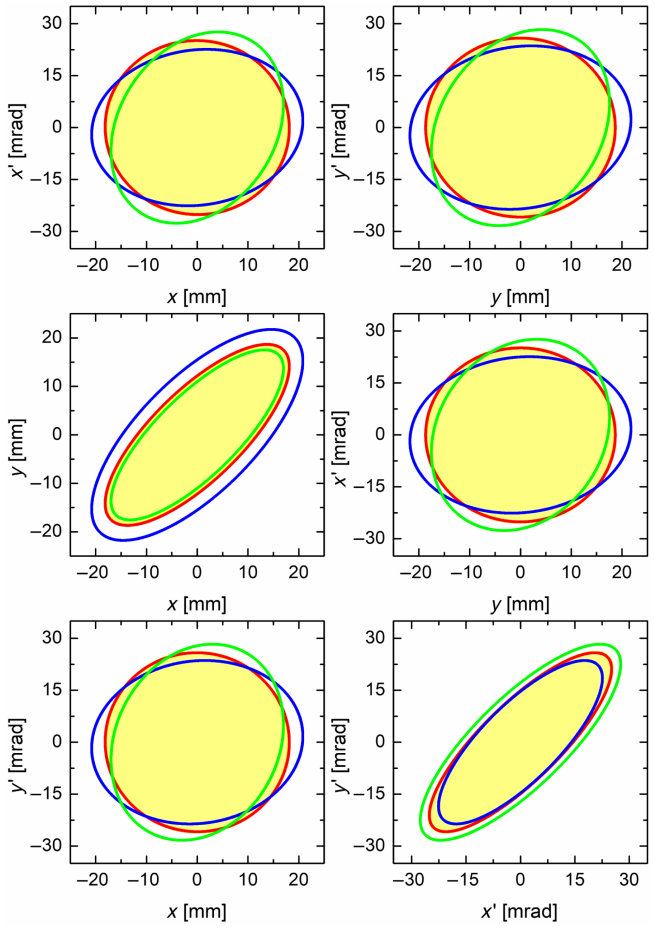


FIG. 9. Projected 4× rms-ellipses at the entrance (yellow) and exit of the first lattice period for an intense coupled coasting proton beam, simulated using the soft-edge approximation at field strengths of 0.24, 0.30, and 0.36 T (blue, red, and green), with entrance ellipses fully enclosed by the corresponding exit ellipses at the nominal field strength.

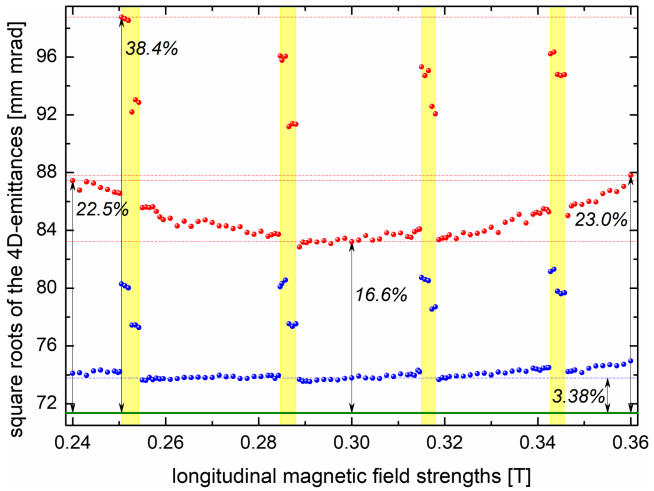


FIG. 10. Square roots of the 4D emittances at the exit of the solenoid channel, obtained using the hard-edge model for both high-current and negligible-current cases (red and blue). The olive line indicates the square root of the 4D emittance at the entrance. The initial Gaussian distribution is rms-equivalent to the beam matrix $\Sigma_{\mathrm{in}}^{\otimes}$ for all field strengths.

solenoid channel. Using the hard-edge model, several unstable regions appear, corresponding to resonance conditions in which the beam mismatch strongly couples to the focusing lattice, resulting in unphysical growth of the 4D emittance due to inadequate representation of the fringe fields. In contrast, employing the more realistic soft-edge model suppresses such unphysical increases, as shown in Fig. 11.

High-current multiparticle tracking simulations without re-matching show a substantial increase in the square root of the 4D emittance: 23% for the hard-edge model at a field strength of 0.36 T, compared with 13% for the soft-edge

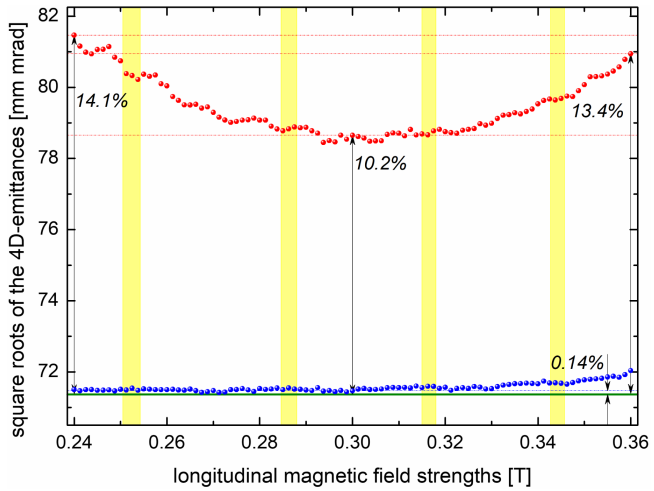


FIG. 11. Conditions are analogous to those illustrated in Fig. 10, with the sole modification being that each solenoid is modeled using the soft-edge approximation.

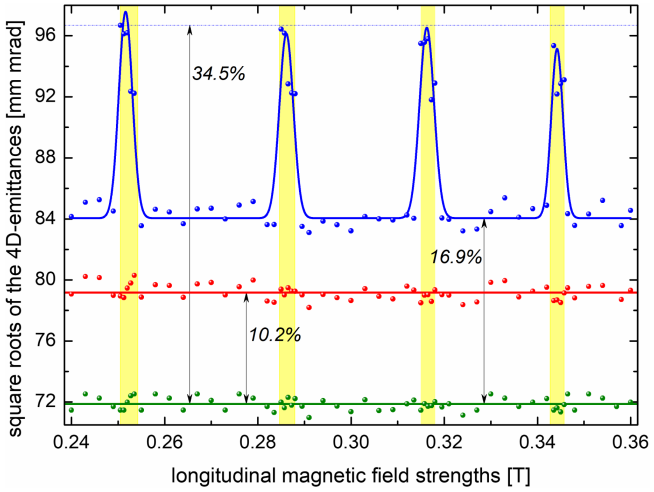


FIG. 12. Square roots of the 4D emittances at the exit of the solenoid channel for optimized intense coupled proton beams. Simulation results obtained using the hard-edge and soft-edge models (blue and red) are compared, with olive dots indicating the corresponding entrance values.

model. It should be emphasized, however, that in the absence of space-charge forces, the 4D emittance remains invariant and is strictly conserved.

At negligible current, simulations show that modeling hard-edge solenoids at the nominal field strength produces an artificial 3.4% increase in the square root of the 4D emittance. This deviation arises from numerical artifacts associated with the discontinuous hard-edge field approximation and from intrinsic limitations of the tracking algorithm. In contrast, if the soft-edge model is employed, the square root of the 4D emittance increases by only 0.1% at the nominal field strength, in full agreement with theoretical expectations. Furthermore, the narrow instability regions observed previously vanish entirely, as illustrated in Fig. 11.

In the subsequent high-current multiparticle tracking simulations, the beam matrix $\Sigma_{\mathrm{in}}^{\otimes}$ is optimized individually for each applied field strength. The resulting dependence of the square root of the 4D emittance at the exit of the solenoid channel on the field strength is shown in Fig. 12.

Using the hard-edge model, the average square root of the 4D emittance increases by 17% at the exit of the periodic solenoid focusing channel (excluding unstable regions), whereas the soft-edge model limits the growth to 10%. This result underscores the importance of realistic field modeling in minimizing artificial emittance growth.

## VIII. MATCHING: ENVELOPE VS MOMENT

In this section, envelope matching is contrasted with rms-moment matching. The objective of envelope matching is to achieve periodicity of the rms-beam sizes, $\mathtt{X}_1$ and $\mathtt{Y}_1$, together with their derivatives, $\mathtt{X}_2$ and $\mathtt{Y}_2$, over a single lattice period. In contrast, rms-moment matching aims to enforce periodicity of all independent rms moments.

A longitudinal magnetic field of 0.30 T is adopted as the nominal field in Figs. 10 and 11, and the corresponding input particle distribution is optimized for this field; consequently, only minimal 4D emittance increase is

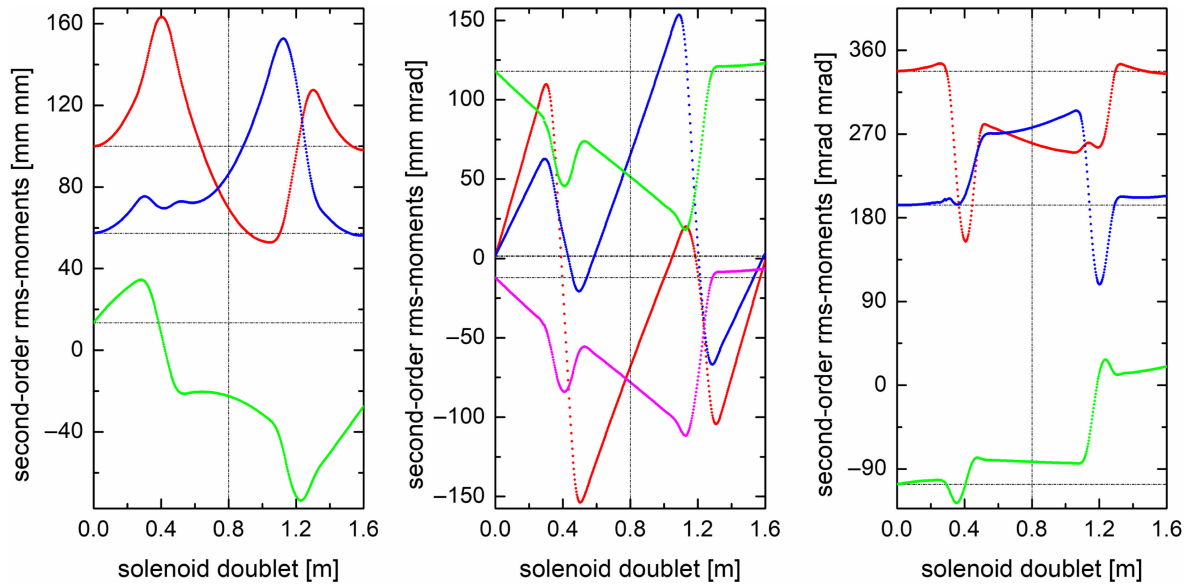


FIG. 13. Particle tracking of an envelope-matched beam: evolution of the ten independent rms moments along the first period for a coupled coasting proton beam (10 mA). The initial Gaussian distribution is rms-equivalent to the beam matrix $\Sigma_{\mathrm{in}}^{\mathrm{2D}}$, with each solenoid operating at a field strength of 0.36 T. Left: $\tilde{\mathtt{X}}_1$, $\tilde{\mathtt{Y}}_1$, and $\tilde{\mathtt{Z}}_1$ (red, blue, and green); middle: $\tilde{\mathtt{X}}_2$, $\tilde{\mathtt{Y}}_2$, $\tilde{\mathtt{Z}}_2$, and $\tilde{\mathtt{Z}}_3$ (red, blue, green, and magenta); right: $\tilde{\mathtt{X}}_3$, $\tilde{\mathtt{Y}}_3$, and $\tilde{\mathtt{Z}}_4$ (red, blue, and green).

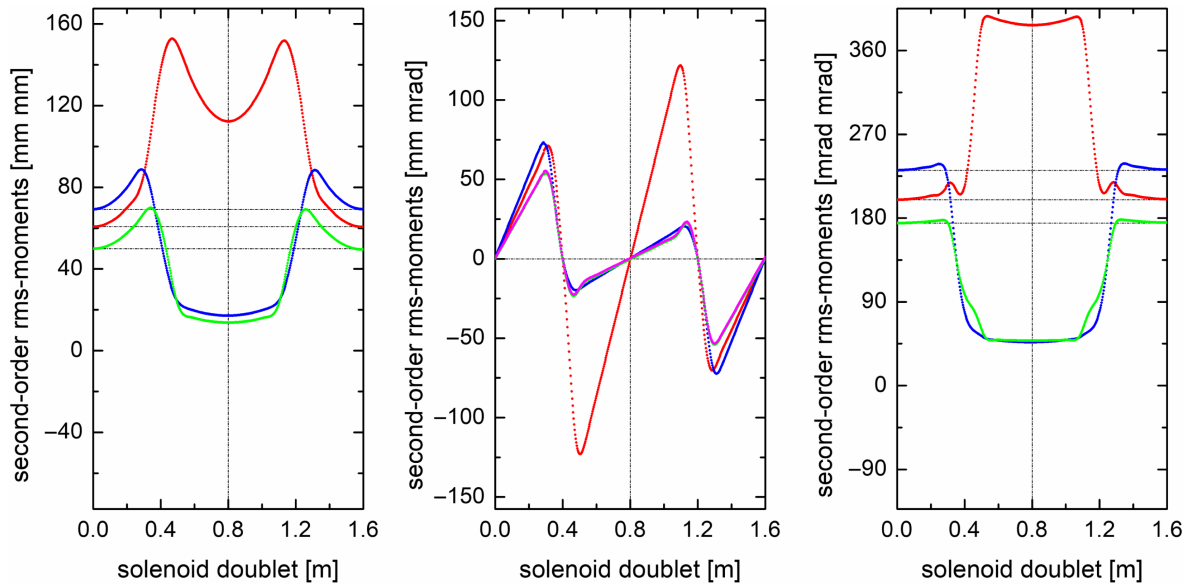


FIG. 14. Particle tracking is performed under conditions similar to those demonstrated in Fig. 13, with the sole modification that the initial Gaussian distribution is constructed to be rms-equivalent to the beam matrix $\Sigma_{\text{in}}^{4D}$.

observed at the nominal field. The objective of Sec. VIII is to demonstrate that rms-moment matching performs significantly better than envelope matching in the periodic solenoid focusing channel. However, at the nominal field, achieving a perfectly envelope-matched input beam matrix is challenging. By increasing the magnetic field to 0.36 T, both a perfectly envelope-matched scenario and an rms-moment-matched scenario can be readily realized, thereby allowing a clearer and more direct comparison between the two matching approaches.

Assuming a solenoid field strength of 0.36 T, the corresponding matched input beam matrices, $\Sigma_{\text{in}}^{2D}$ and $\Sigma_{\text{in}}^{4D}$, are given below (in units of mm and mrad)

$$\Sigma_{\text{in}}^{2D} = \begin{bmatrix} +100.9 & +0.256 & +13.16 & +119.4 \\ \cdots & +340.7 & -12.10 & -108.8 \\ \cdots & \cdots & +57.52 & +0.866 \\ \cdots & \cdots & \cdots & +196.5 \end{bmatrix} \tag{76}$$

and

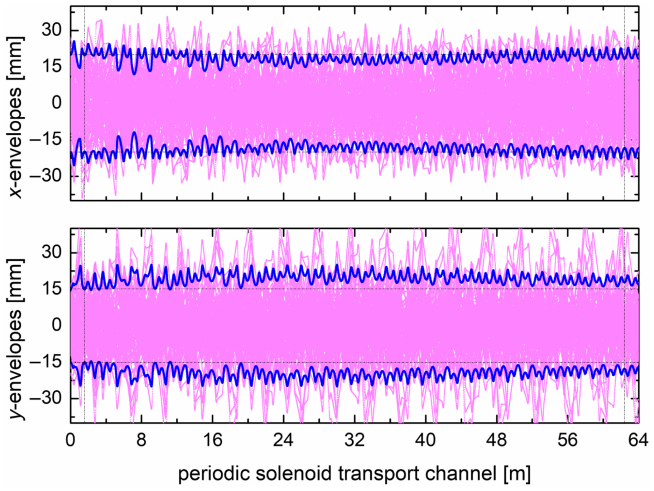


FIG. 15. Horizontal and vertical 2× rms-beam sizes, together with representative particle trajectories for an intense coupled coasting proton beam. The initial Gaussian distribution, rms-equivalent to the matrix $\Sigma_{\text{in}}^{2D}$, is defined as envelope-matched. Each solenoid is modeled using the soft-edge approximation at a field strength of 0.36 T.

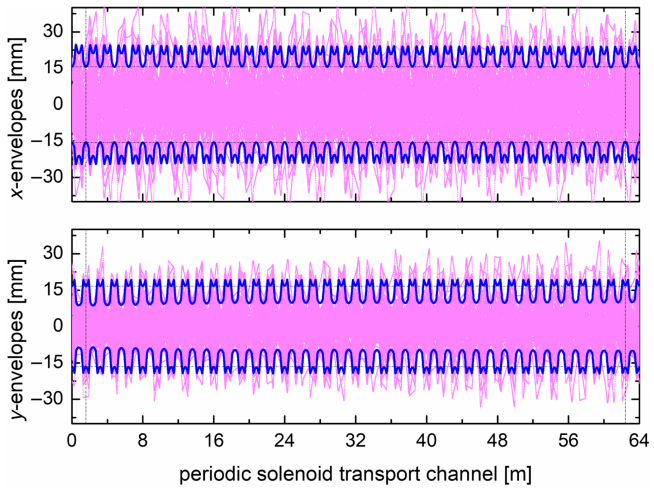


FIG. 16. Setup is analogous to that shown in Fig. 15, with the difference that the initial Gaussian distribution is defined to be rms-moment-matched and rms-equivalent to the beam matrix $\Sigma_{\text{in}}^{4D}$.

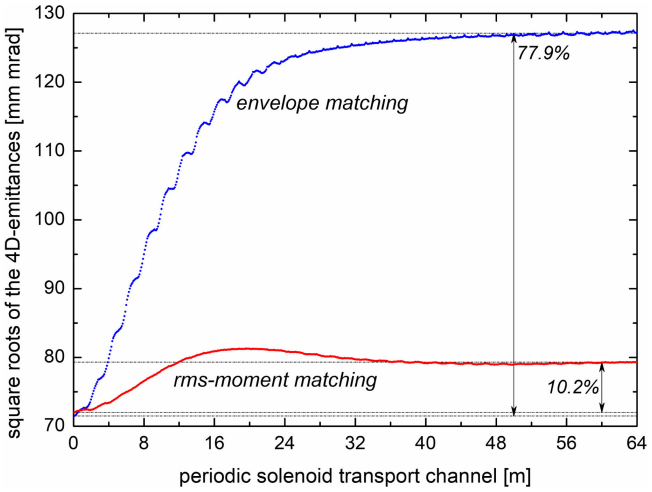


FIG. 17. Square roots of the 4D emittances, $\sqrt{\varepsilon_{4D}}$, along the periodic solenoid focusing channel at a field strength of 0.36 T, obtained from multiparticle tracking simulations using the soft-edge approximation. The blue and red curves correspond to initial Gaussian distributions rms-equivalent to the beam matrices $\Sigma_{\mathrm{in}}^{2D}$ and $\Sigma_{\mathrm{in}}^{4D}$, respectively.

$$\Sigma_{\mathrm{in}}^{4D} = \begin{bmatrix} +60.85 & +0.109 & +49.94 & +0.037 \\ \cdots & +199.6 & +0.066 & +175.6 \\ \cdots & \cdots & +69.03 & +0.043 \\ \cdots & \cdots & \cdots & +232.5 \end{bmatrix}. \quad (77)$$

The beam matrix, $\Sigma_{\mathrm{in}}^{2D}$, defines an rms-size-matched particle distribution at the entrance of the solenoid focusing channel. The evolution of all rms moments over the first lattice period, obtained from multiparticle tracking, is shown in Fig. 13. Strict periodicity is observed for the beam sizes and slopes, whereas the projected phase-space planes involving interplane coupling do not exhibit periodicity, indicating that envelope matching alone cannot account for correlations between planes. In contrast, the beam matrix, $\Sigma_{\mathrm{in}}^{4D}$, incorporates the full set of interplane correlations, ensuring that all rms moments are preserved from period to period, as illustrated in Fig. 14.

The horizontal and vertical 2× rms-beam sizes through the periodic solenoid focusing channel, calculated using envelope matching and rms-moment matching, are shown in Figs. 15 and 16, respectively.

If envelope matching is applied, the 2× rms-beam sizes do not exhibit proper periodicity along the solenoid channel. Multiparticle tracking simulations confirm that, under envelope matching, the square root of the 4D emittance increases rapidly along the solenoid focusing channel.

In contrast, full 4D rms-moment matching ensures that all ten independent rms moments are exactly reproduced from period to period. This approach enforces strict periodicity of the beam envelopes, effectively suppresses envelope oscillations, and mitigates the impact of nonlinear space-charge forces. Multiparticle tracking simulations confirm that, under rms-moment matching, the square root of the 4D emittance is significantly better preserved, as illustrated in Fig. 17.

An increase in the projected emittances, without a corresponding increase in the eigenemittances, reflects interplane coupling rather than a genuine degradation of beam quality, whereas an increase in the eigenemittances indicates an actual loss of intrinsic beam brightness.

Transporting the beam through the periodic solenoid focusing channel using rms-moment matching results in a 10% increase in the square root of the 4D emittance. In contrast, employing envelope matching leads to a 78%

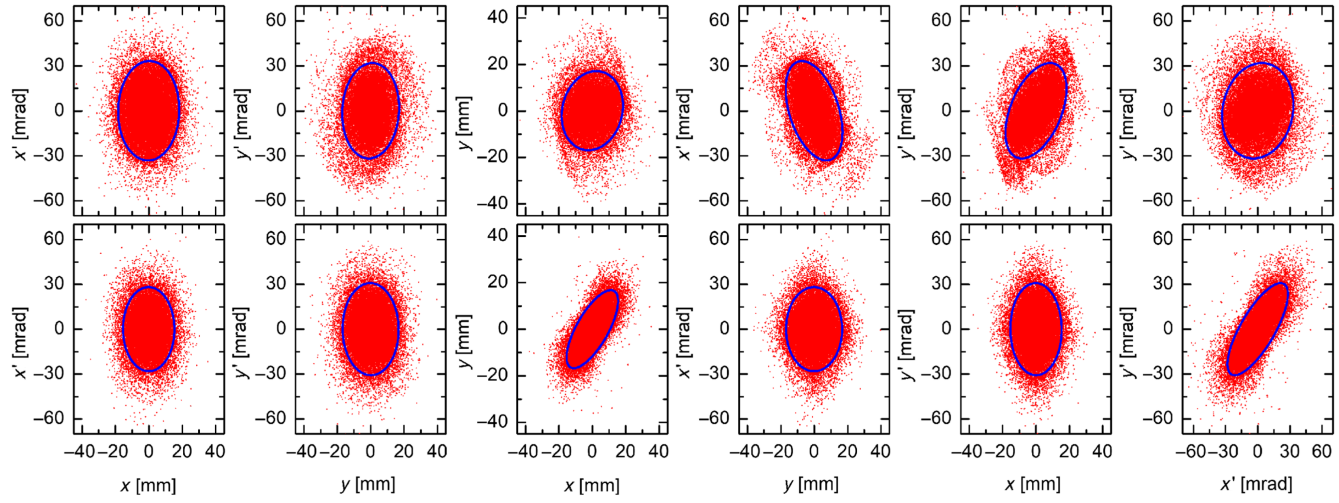


FIG. 18. Particle distributions at the exit of the solenoid focusing channel projected onto six phase-space subplanes for envelope matching (top; initial Gaussian distribution rms-equivalent to the beam matrix $\Sigma_{\mathrm{in}}^{2D}$) and rms-moment matching (bottom; initial Gaussian distribution rms-equivalent to the beam matrix $\Sigma_{\mathrm{in}}^{4D}$). Soft-edge solenoids are operated at the field strength of 0.36 T. The corresponding transverse eigenemittances are evaluated as 76.61/211.0 and 30.47/206.5 mm mrad for the top and bottom cases, respectively.

increase, clearly demonstrating the significant advantage of rms-moment matching. The corresponding particle distributions at the exit of the channel are shown in Fig. 18.

## IX. CONCLUSION

There is increasing interest in the use of coupled beams as a promising approach to achieve higher luminosities and enhanced beam brightness in high-intensity accelerator applications. In the periodic solenoid focusing channel with alternating polarities considered in this study, widely used optics codes such as Trace-2D [19] provide numerical matching routines for uncoupled beams, allowing the determination of periodic solutions that include linearized space-charge forces. To the best of our knowledge, however, no general numerical matching routine is currently available for intense coupled beams.

In this paper, several rms-moment-matched transport solutions exhibiting substantial interplane coupling are derived analytically for a periodic solenoid focusing channel with alternating polarities. Particle tracking simulations, performed along this channel using the Beampath code, confirm that the proposed rms-moment matching formalism remains accurate and robust even in the presence of strong nonlinear space-charge forces.

The transverse beam envelopes are found to be largely insensitive to the detailed structure of the solenoid fringe fields. Both hard-edge and soft-edge solenoids at a given field strength yield nearly identical envelopes (simulated but not shown). In contrast, the increase in the square root of the 4D emittance is strongly influenced by the longitudinal magnetic field profile: hard-edge solenoids consistently overestimate emittance growth relative to more realistic soft-edge representations.

In summary, the present study establishes rms-moment matching as a rigorous and practical framework for the analysis and control of intense coupled coasting proton beams in periodic solenoid focusing channels with alternating polarities. The approach provides a robust foundation for beam matching and transport design in modern accelerator systems, particularly those employing superconducting solenoids integrated with superconducting radio-frequency cavities for the acceleration of high-intensity proton and heavy-ion beams.

## DATA AVAILABILITY

The data are not publicly available. The data are available from the authors upon reasonable request.

## APPENDIX A: ANALYTICAL PERIODIC SOLUTIONS FOR SOLENOID DOUBLETS WITH LINEARIZED SPACE-CHARGE FORCES

The beamline used to establish a periodic solution for the solenoid doublet is conceptually divided into two sections: a matching section $\mathfrak{R}$, which transforms the initial uncoupled beam into a configuration suitable for periodic transport without considering space-charge effects, and a periodic solenoid doublet $\mathfrak{I}_{\rm sc}(\aleph)$. The region between $z_0$ and $z_1$ defines the matching section, whereas the interval from $z_1$ to $z_2$ corresponds to the periodic solenoid doublet.

At the entrance of the beamline (position $z_0$), the beam is assumed to be initially uncoupled, with its phase-space properties described by the sigma matrix of transverse second-order moments of the particle distribution,

$$\Sigma(z_0) = \Sigma = \begin{bmatrix} \Sigma_{xx} & \Sigma_{xy} \\ \Sigma_{xy}^{\rm T} & \Sigma_{yy} \end{bmatrix}, \qquad \Sigma_{xy} = \begin{bmatrix} 0 & 0 \\ 0 & 0 \end{bmatrix}, \quad \text{(A1)}$$

where $\Sigma_{xx}$ and $\Sigma_{yy}$ are the $2\times 2$ transverse submatrices associated with the horizontal and vertical planes, respectively.

Figure 19 schematically illustrates the beamline configuration used to determine the periodic solution of a proton beam in a periodic solenoid channel.

The uncoupled beam matrix at the entrance of the matching section is assumed to take the form (in units of mm and mrad)

$$\Sigma = \begin{bmatrix} +207.5 & -350.0 & 0 & 0 \\ \cdots & +593.2 & 0 & 0 \\ \cdots & \cdots & +164.7 & +105.0 \\ \cdots & \cdots & \cdots & +341.2 \end{bmatrix}, \quad \text{(A2)}$$

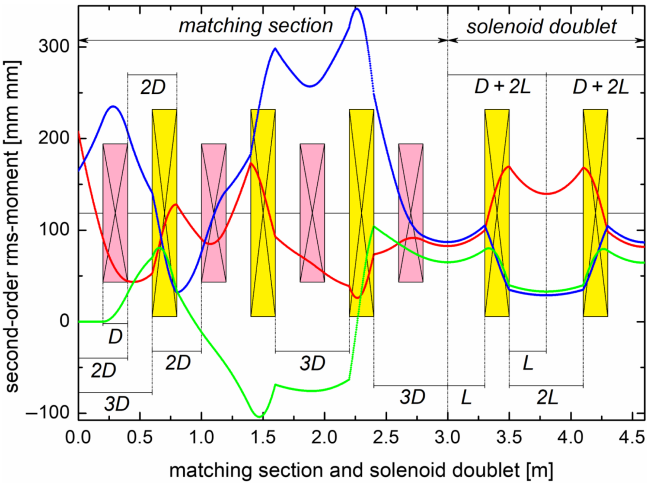


FIG. 19. Schematic overview of the beamline configuration. Solenoids and rotated quadrupoles are represented by yellow and rose blocks, respectively. The red, blue, and green curves denote the second moments X1, Y1, and $Z_1$, obtained from rms tracking. Space-charge effects are neglected throughout the matching section. The effective lengths of the solenoids and rotated quadrupoles, as well as the separations between adjacent elements, are all denoted by $D$. The field gradients of the rotated quadrupoles are −0.649, −0.603, 0.153, and 0.340 T/m, with corresponding rotation angles of 14.37, 1.229, −0.093, and 0.596°. The solenoid field strength is set to its nominal value of 0.30 T.

and the corresponding transport matrix of the matching section under full space-charge compensation is (in units of m and rad)

$$\Re(\aleph) = \begin{bmatrix} -0.824 & -0.359 & +0.447 & -0.504 \\ -3.806 & -2.287 & +0.835 & +0.137 \\ +0.792 & +0.345 & +0.462 & -0.522 \\ +3.678 & +2.210 & +0.867 & +0.142 \end{bmatrix}. \quad \text{(A3)}$$

In the zero-current limit, the effective focusing forces of the solenoid doublet are determined exclusively by the external lattice and are consequently independent of the beam shape or orientation. Under these conditions, the periodic solution can be obtained analytically, even in the presence of full transverse coupling. In contrast, for high-current beams transported through the solenoid doublet, the defocusing space-charge forces depend on the beam real-space shape and orientation. Because rms-equivalent KV distributions have been demonstrated to accurately reproduce these linearized space-charge forces in transverse matching studies, the present analysis adopts an rms-based KV modeling approach.

The periodic solution of the beam in the zero-current limit is determined by the self-consistency condition

$$\Sigma_{\text{in}} = \Sigma(z_1) \approx \Im \cdot \Sigma(z_1) \cdot \Im^{\text{T}} = \Sigma_{\text{out}}, \quad \text{(A4)}$$

the overall transfer matrix from the entrance of the beamline to the exit of the solenoid doublet is then given by

$$\mho(\aleph) = \Im \cdot \Re(\aleph), \quad \text{(A5)}$$

where $\Re(\aleph)$ represents the matching transformation, parameterized by the set of adjustable matching parameters contained in $\aleph$. The transport matrix $\Im$ is assumed to be fully known, as it depends solely on the lattice configuration of the solenoid doublet.

From first principles, neither the periodic solution nor the elements of $\aleph$, which define the appropriate matching transformation from the entrance of the beamline to the entrance of the solenoid doublet, are known *a priori*.

The iterative procedure used to determine both quantities begins with an initial guess, $\aleph'(\mathtt{m}_1, \mathtt{m}_2, \cdots \mathtt{m}_{16})$, which satisfies the symplecticity condition. However, this initial estimate generally does not fulfill the periodicity requirement, i.e.,

$$\Re(\aleph') \cdot \Sigma \cdot \Re^{\text{T}}(\aleph') \neq \mho(\aleph') \cdot \Sigma \cdot \mho^{\text{T}}(\aleph'), \quad \text{(A6)}$$

so that the beam matrix at the entrance of the solenoid focusing channel does not reproduce itself after transport through the first lattice cell.

Using the Mathcad subroutine `Minerr`, a set of matching parameters $\aleph^{\text{o}}$ can be determined for the zero-current configuration, such that the symplectic condition is exactly satisfied and periodicity is simultaneously enforced. This subroutine is developed to solve under-determined systems of equations subject to a prescribed set of boundary conditions. In this context, the algorithm iteratively adjusts the components of the matching matrix $\Re(\aleph^{\text{o}})$ to minimize the residual error between the input beam matrix at the solenoid doublet entrance and the output beam matrix obtained by transporting $\Sigma$ through the matching section $\Re(\aleph^{\text{o}})$ and the solenoid doublet $\Im$

$$\Re(\aleph^{\text{o}}) \cdot \Sigma \cdot \Re^{\text{T}}(\aleph^{\text{o}}) \approx \mho(\aleph^{\text{o}}) \cdot \Sigma \cdot \mho^{\text{T}}(\aleph^{\text{o}}), \quad \text{(A7)}$$

which ensures that the beam matrix at the entrance of the solenoid doublet closely reproduces itself after a single lattice cell. Once $\aleph^{\text{o}}$ is determined, the periodic beam solution at the entrance of the solenoid doublet can then be obtained by transporting the initial beam matrix through the matching section $\Re(\aleph^{\text{o}})$.

For KV beams, the electric self-field generated by space charge can be evaluated analytically, as originally derived by Sacherer [2] for uncoupled coasting beams, i.e., beams with upright elliptical cross sections in real space. In the presence of interplane coupling, the rms-ellipse is generally tilted with respect to the laboratory axes, as plotted in Fig. 20. In this situation, the space-charge forces are first computed in the tilted frame, aligned with the principal axes of the ellipse, and then transformed back into the upright laboratory frame for incorporation into the beam dynamics. This effect is equivalent to a defocusing quadrupole kick in both transverse planes. Although the effective defocusing strengths differ along the two principal directions, the resulting 4D transformation remains symplectic. Consequently, the space-charge contribution can be represented as an additional space-charge kick matrix $\tau$.

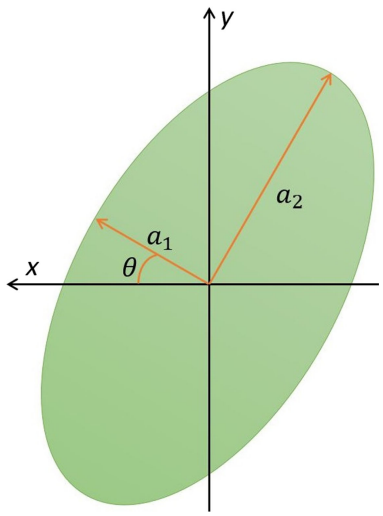


FIG. 20. Ellipse of an $x-y$ coupled beam in real space. $\mathcal{A}_{xy}$ denotes the rms area, see Eq. (A8), while $\alpha_{xy}$ and $\beta_{xy}$ are the equivalent Twiss parameters that define the orientation and aspect ratio of the rms-ellipse. The $x$, $y$, and $z$ unit vectors of the Cartesian coordinate system follow the right-hand rule.

The rms-ellipse in real space is defined by its semiaxes $a_1$ and $a_2$ and by the rotation angle $\theta$ of $a_1$ relative to $x$ axis. Its rms area is given by

$$\mathcal{A}_{xy} = \sqrt{\mathtt{X}_1\mathtt{Y}_1 - \mathtt{Z}_1^2} = a_1 \cdot a_2. \tag{A8}$$

The equivalent Twiss parameters can be expressed in terms of the beam moments as

$$\beta_{xy} = \frac{\mathtt{X}_1}{\mathcal{A}_{xy}}, \qquad \alpha_{xy} = -\frac{\mathtt{Z}_1}{\mathcal{A}_{xy}}, \tag{A9}$$

and the dimensionless auxiliary quantity is defined as

$$\mathcal{H} = \frac{\beta_{xy}}{2} + \frac{1+\alpha_{xy}^2}{2\beta_{xy}}. \tag{A10}$$

The semiaxes of the rms-ellipse are then obtained from

$$a_{1,2} = \sqrt{\frac{\mathcal{A}_{xy}}{2}} \cdot \left(\sqrt{\mathcal{H}+1} \pm \sqrt{\mathcal{H}-1}\right), \tag{A11}$$

where the plus sign corresponds to the major semiaxis $a_2$ and the minus sign to the minor semiaxis $a_1$.

The rotation angle $\theta$ of the rms-ellipse relative to the $x$ axis is determined from the equivalent Twiss parameters according to

$$\theta = \frac{1}{2}\arctan\left(\frac{-2\alpha_{xy}}{\beta_{xy} - \frac{1+\alpha_{xy}^2}{\beta_{xy}}}\right). \tag{A12}$$

The space-charge transfer matrix $\tau$ is constructed according to

$$\tau = [M^{\rightarrow}_{\text{rotation}}(\theta)]^{-1} \cdot \tau^{\circlearrowleft} \cdot M^{\rightarrow}_{\text{rotation}}(\theta), \tag{A13}$$

where $\tau^{\circlearrowleft}$ is the space-charge transfer matrix expressed in the frame aligned with the principal axes of the rms-ellipse.

In the principal-axis frame, the space-charge transfer matrix is diagonal and can be written as

$$\tau^{\circlearrowleft} = \begin{bmatrix} \tau^{\circlearrowleft}_{a_1} & 0 \\ 0 & \tau^{\circlearrowleft}_{a_2} \end{bmatrix}, \qquad \tau^{\circlearrowleft}_{a_1,a_2} = \begin{bmatrix} 1 & 0 \\ \kappa_{a_1,a_2} \cdot \delta_z & 1 \end{bmatrix}, \tag{A14}$$

where $\delta_z$ denotes the longitudinal step size between consecutive space-charge kicks. The quantities $\kappa_{a_1}$ and $\kappa_{a_2}$ describe the effective defocusing strengths along the respective semiaxis of the rms-ellipse and are defined by

$$\kappa_{a_1} = \frac{\kappa_{\text{sc}}}{2a_1(a_1+a_2)}, \qquad \kappa_{a_2} = \frac{\kappa_{\text{sc}}}{2a_2(a_1+a_2)}, \tag{A15}$$

with the generalized beam perveance defined as

$$\kappa_{\text{sc}} = \frac{qI}{2\pi\epsilon_0 m(\gamma\beta c)^3}. \tag{A16}$$

With these prerequisites, any beamline composed of solenoids transporting a coupled high-intensity beam can be modeled as a sequence of symplectic transport matrices. Each solenoid and drift section is subdivided into multiple slices, and the beam is propagated through each slice over the longitudinal step $\delta_z$ using the standard slice transport matrix, neglecting space-charge forces. At the end of each integration step $\delta_z$, the effect of space charge is incorporated via the corresponding symplectic kick, $\tau$. In this way, the complete evolution of the coupled, space-charge-dominated beam is accurately represented as an alternating sequence of linear transport and space-charge kicks. Within our numerical subroutine, the parameters $a_{1,2}$ and $\theta$ are recalculated and updated immediately preceding the space-charge kick, using the local beam matrix evaluated at the corresponding longitudinal position $z$.

The iterative procedure to obtain a periodic solution at finite beam current begins with the initial beam matrix $\Sigma$ propagated through the matching section $\Re(\aleph^{\circ})$, which is optimized for zero beam current. The resulting matched (periodic) beam matrix at the entrance of the solenoid doublet is

$$\Sigma^{\circ}_{\text{in}} = \Re(\aleph^{\circ}) \cdot \Sigma \cdot \Re^{\text{T}}(\aleph^{\circ}), \tag{A17}$$

and serves as the starting point for the subsequent high-current iteration. It should be noted that

$$\Sigma^{\circ}_{\text{in}} \approx \Im \cdot \Re(\aleph^{\circ}) \cdot \Sigma \cdot \Re^{\text{T}}(\aleph^{\circ}) \cdot \Im^{\text{T}}, \tag{A18}$$

where the zero-current matrix $\Im$ is independent of $\aleph^{\circ}$ and differs from the high-current matrix $\Im_{\text{sc}}(\aleph^{\circ})$.

The beam matrix is then propagated through a single lattice cell at the intended beam current. From this high-current tracking, the transport matrix of a single lattice cell, $\Im_{\text{sc}}(\aleph^{\circ})$, is obtained. By construction, $\Im_{\text{sc}}(\aleph^{\circ})$ depends both on the beam current and on the spatial beam parameters at the entrance of the solenoid focusing channel. The resulting 16 elements of $\Im_{\text{sc}}(\aleph^{\circ})$ are stored for subsequent use. In general, the initial beam matrix $\Sigma$ does not satisfy the condition for the periodic solution at finite beam current, i.e.,

$$\Sigma^{\circ}_{\text{in}} \neq \Im_{\text{sc}}(\aleph^{\circ}) \cdot \Re(\aleph^{\circ}) \cdot \Sigma \cdot \Re^{\text{T}}(\aleph^{\circ}) \cdot \Im^{\text{T}}_{\text{sc}}(\aleph^{\circ}). \tag{A19}$$

However, the cell transfer matrix $\Im_{\text{sc}}(\aleph^{\circ})$ is then used to update the matching setting, producing a new matching matrix $\Re(\aleph^{1})$ that ensures the beam matrix is identical before and after transport through the lattice cell, i.e.,

$$\Sigma^{1}_{\text{in}} \approx \Im_{\text{sc}}(\aleph^{\circ}) \cdot \Re(\aleph^{1}) \cdot \Sigma \cdot \Re^{\text{T}}(\aleph^{1}) \cdot \Im^{\text{T}}_{\text{sc}}(\aleph^{\circ}), \tag{A20}$$

emphasizing that this relation explicitly utilizes the previously stored elements of $\mathfrak{I}_{sc}(\aleph^0)$; however, noting that $\mathfrak{I}_{sc}(\aleph^0)$ is distinct from $\mathfrak{I}_{sc}(\aleph^1)$.

The updated transfer matrix $\mathfrak{R}(\aleph^1)$ delivers the beam matrix $\Sigma_{in}^1$ at the entrance of the solenoid focusing channel. This beam matrix is then propagated through a single lattice cell at finite beam current, producing a new cell transfer matrix $\mathfrak{I}_{sc}(\aleph^1)$. Similarly, the resulting $\mathfrak{I}_{sc}(\aleph^1)$ is stored and used to readjust the matching, generating a new setting $\aleph^2$ that satisfies the periodicity condition under the updated lattice configuration defined by $\aleph^1$

$$\Sigma_{in}^2 \approx \mathfrak{I}_{sc}(\aleph^1) \cdot \mathfrak{R}(\aleph^2) \cdot \Sigma \cdot \mathfrak{R}^T(\aleph^2) \cdot \mathfrak{I}_{sc}^T(\aleph^1). \tag{A21}$$

This, in turn, provides a new beam matrix $\Sigma_{in}^2$ at the entrance of the solenoid focusing channel, which leads to the corresponding updated cell transfer matrix $\mathfrak{I}_{sc}(\aleph^2)$. Repeating this procedure causes the sequence of matching parameters to converge, such that the change between successive iterations, from $\aleph^n$ to $\aleph^{n+1}$, becomes progressively smaller and eventually negligible. After a sufficient number of iterations $J$, the periodicity condition is satisfied to the prescribed accuracy, such that

$$\Sigma_{in}^J \approx \mathfrak{I}_{sc}(\aleph^J) \cdot \mathfrak{R}(\aleph^J) \cdot \Sigma \cdot \mathfrak{R}^T(\aleph^J) \cdot \mathfrak{I}_{sc}^T(\aleph^J). \tag{A22}$$

and the corresponding periodic solution for the coupled, space-charge-dominated beam is obtained.

The matrix $\Sigma_{in}^J$ contains the periodic second-order moments at the entrance of the solenoid focusing channel, while $\mathfrak{I}_{sc}(\aleph^J)$ denotes the corresponding transfer matrix of a single lattice cell, incorporating the effects of beam current and interplane coupling. Since each $\mathfrak{I}_{sc}(\aleph^n)$ is constructed as a product of symplectic slice matrices, all transport matrices in the iteration sequence remain symplectic. As a direct consequence, each $\Sigma_{in}^n$ preserves the eigenemittances throughout the iterative procedure.

## APPENDIX B: DERIVATION OF MATCHED BEAM CONDITIONS WITHOUT AND WITH LINEARIZED SPACE-CHARGE FORCES

In the following, we present the derivation of Eqs. (46) and (47), which neglect space-charge effects. The derivations of Eqs. (54)–(61), which include linear space-charge effects, proceed analogously and employ the same arguments and methods. In all cases, the procedure is identical and consists of the following steps: (i) Apply the general transport law for the second-order beam-moments matrix. (ii) Exploit the symmetry of the input beam matrix. (iii) Require that the beam matrix remain unchanged before and after transport through the periodic matrix $\mathfrak{I}$. (iv) Incorporate the physical characteristics of the periodic solution for the initial beam matrix $\Sigma_{in}$. (v) Expand the matrix equation obtained in the first step into a set of equations relating the individual matrix elements.

These steps are illustrated using a fully $x-y$ coupled particle distribution with negligible current, leading to Eqs. (46) and (47).

Step 1: Begin with Eq. (A4), which describes the transport of the coupled beam matrix $\Sigma_{in}^{\odot}$ through the zero-current transport matrix $\mathfrak{I}^{\odot}$. Here, "in" refers to the beam matrix upstream of $\mathfrak{I}^{\odot}$, while "out" denotes the beam matrix downstream.

Step 2: Both $\mathfrak{I}^{\odot}$ and $\Sigma_{in}^{\odot}$ are $4\times 4$ matrices. The beam matrix $\Sigma_{in}^{\odot}$ is symmetric because any second-order moment, e.g., $\langle xx'\rangle$, equals $\langle x'x\rangle$. Consequently, $\Sigma_{in}^{\odot}$ contains ten independent elements. The transport matrix $\mathfrak{I}^{\odot}$ is symplectic and therefore has unit determinant. By definition,

$$\det(\mathfrak{I}^{\odot}) = \mathtt{A}_1^2 - \mathtt{A}_2\mathtt{B}_2 = 1, \tag{B1}$$

as stated in Eq. (48).

Step 3: For a periodic solution, the beam matrix is identical before and after transport. Denoting this common matrix by $\Sigma_{in}^{\odot}$, Eq. (A4) reduces to

$$\Sigma_{in}^{\odot} = \mathfrak{I}^{\odot} \cdot \Sigma_{in}^{\odot} \cdot (\mathfrak{I}^{\odot})^T. \tag{B2}$$

Step 4: Consider Eq. (43). A periodic solution reflects the lattice periodicity and exhibits extrema of the beam sizes both at the center of the focusing element (here, the solenoid) and at the center of the drift space. Since

$$\frac{d}{dz}\langle x^2\rangle = 2\left\langle x\cdot\frac{dx}{dz}\right\rangle := 0, \tag{B3}$$

it follows that $\langle xx'\rangle = \langle yy'\rangle = 0$ at this location. Using the definitions $\mathtt{X}_2 = \langle xx'\rangle$ and $\mathtt{Y}_2 = \langle yy'\rangle$, Eq. (43) summarizes these conditions and is applied in the second and fifth statements of Eq. (46).

Step 5: The equation in Step 3 involves $4\times 4$ matrices and is therefore equivalent to 16 scalar equations. However, the symmetry of $\Sigma$ reduces these to ten independent equations, which can be written explicitly. For example, the first equation reads

$$\mathtt{X}_1 = \mathtt{A}_1^2 \cdot \mathtt{X}_1 + \mathtt{A}_2\mathtt{B}_2 \cdot \mathtt{X}_2, \tag{B4}$$

which corresponds to the first relation in Eq. (46). Similarly,

$$\mathtt{X}_2 = \mathtt{A}_1\mathtt{B}_1 \cdot \mathtt{X}_1 + \mathtt{A}_1\mathtt{A}_2 \cdot \mathtt{X}_3, \tag{B5}$$

which yields the second relation in Eq. (46). Applying the same procedure to the remaining elements of $\Sigma_{in}^{\odot}$ directly produces the complete set of relations given in Eqs. (46) and (47).

The same five steps, together with straightforward algebra, yield all equations in Secs. V A–V C. The differences arise only from the specific properties of the periodic solution and the associated beam-transport matrix introduced at the beginning of each subsection. Applying this procedure yields the matched input beam matrices $\Sigma_{in}^{\odot}$,

$\Sigma_{\mathrm{in}}^{\oplus}$, and $\Sigma_{\mathrm{in}}^{\otimes}$, together with their corresponding transport matrices $\mathfrak{I}^{\odot}$, $\mathfrak{I}_{\mathrm{sc}}^{\oplus}$, and $\mathfrak{I}_{\mathrm{sc}}^{\otimes}$.

For the case $\mathtt{X}_2 = \mathtt{Y}_2 = 0$ (i.e., $\alpha_x = \alpha_y = 0$, corresponding to a parallel beam) and negligible beam current, one obtains: $\mathtt{A}_1 = \mathtt{B}_2 = \mathtt{C}_3 = \mathtt{D}_4$, $\mathtt{A}_2 = \mathtt{C}_4$, $\mathtt{B}_1 = \mathtt{D}_3$, $\mathtt{A}_3 = \mathtt{A}_4 = \mathtt{B}_3 = \mathtt{B}_4 = 0$, and $\mathtt{C}_1 = \mathtt{C}_2 = \mathtt{D}_1 = \mathtt{D}_2 = 0$, consistent with Eq. (32). Under these conditions, the analytical periodic solution for one lattice period (Eqs. (23)–(25) in Ref. [9]) reduces to Eq. (46), corresponding to a fully coupled matched beam $\Sigma_{\mathrm{in}}^{\odot}$ with nonzero $\mathtt{Z}_1$, $\mathtt{Z}_2$, $\mathtt{Z}_3$, and $\mathtt{Z}_4$.

Equations (32) and (33) provide explicit expressions for the zero-current transfer matrix of a solenoid doublet with alternating polarities, $\mathfrak{I}^{\odot}$, directly in terms of the lattice parameters. As noted above, when space-charge effects are included, an analytical expression for the transfer matrix is no longer attainable, since the space-charge-modified matrices, $\Sigma_{\mathrm{in}}^{\oplus}$ and $\Sigma_{\mathrm{in}}^{\otimes}$, depend on the initial second moments $\mathtt{X}_1$, $\mathtt{Y}_1$, and $\mathtt{Z}_1$.

When space-charge effects are included and the initial beam is assumed to be fully uncoupled, the conditions: $\mathtt{Z}_1 = \mathtt{Z}_2 = \mathtt{Z}_3 = \mathtt{Z}_4 = 0$ must be satisfied, while $\mathtt{A}_3 = \mathtt{A}_4 = \mathtt{B}_3 = \mathtt{B}_4 = 0$ and $\mathtt{C}_1 = \mathtt{C}_2 = \mathtt{D}_1 = \mathtt{D}_2 = 0$ remain valid. Under these conditions, the analytical periodic solution for a single cell reduces to Eq. (54), describing a matched, uncoupled beam $\Sigma_{\mathrm{in}}^{\oplus}$ with $\mathtt{X}_2 = \mathtt{Y}_2 = 0$. In this case, one also observes that $\mathtt{A}_1 = \mathtt{B}_2$ and $\mathtt{C}_3 = \mathtt{D}_4$.

For a partially coupled high-current beam, $\Sigma_{\mathrm{in}}^{\otimes}$ is characterized by $\mathtt{Z}_2 = \mathtt{Z}_3 = 0$, while $\mathtt{Z}_1$ and $\mathtt{Z}_4$ remain nonzero. In this case, the analytical periodic solution for a single cell reduces to Eqs. (60) and (61), which describe a partially coupled beam with $\mathtt{X}_2 = \mathtt{Y}_2 = 0$. The coupled elements of the transfer matrix are nonzero, namely $\mathtt{A}_3, \mathtt{A}_4, \mathtt{B}_3, \mathtt{B}_4, \mathtt{C}_1, \mathtt{C}_2, \mathtt{D}_1$, and $\mathtt{D}_2$. In this situation, the relations $\mathtt{A}_1 = \mathtt{B}_2$ and $\mathtt{C}_3 = \mathtt{D}_4$ are also satisfied.


[1] M. Reiser, *Theory and Design of Charged Particle Beams* (John Wiley & Sons Inc., New York, 1994).

[2] F. Sacherer, RMS envelope equations with space charge, IEEE Trans. Nucl. Sci. **18**, 1105 (1971).

[3] T. P. Wangler, *Rf Linear Accelerators*, 2nd ed. (Wiley-VCH, Mannheim/Germany, 2008), p. 296.

[4] L. Groening, W. Barth, W. Bayer, G. Clemente, L. Dahl, P. Forck, P. Gerhard, I. Hofmann, G. Riehl, and S. Yaramyshev, Benchmarking of measurement and simulation of transverse rms-emittance growth, Phys. Rev. ST Accel. Beams **11**, 094201 (2008).

[5] L. Groening, M. Maier, C. Xiao, L. Dahl, P. Gerhard, O. K. Kester, S. Mickat, H. Vormann, and M. Vossberg, Experimental proof of adjustable single-knob ion beam emittance partitioning, Phys. Rev. Lett. **113**, 264802 (2014).

[6] D.-O. Jeon, Experimental evidence of space charge driven resonances in high intensity linear accelerators, Phys. Rev. Accel. Beams **19**, 010101 (2016).

[7] L. Arnaudon *et al.*, Linac4 technical design report, Report No. CERN-AB-2006-084-ABP/RF, Geneva, 2006.

[8] A. Khan, O. Boine-Frankenheim, F. Hug, and C. Stoll, Beam matching with space charge in energy recovery linacs, Nucl. Instrum. Methods Phys. Res., Sect. A **948**, 162822 (2019).

[9] C. Xiao and L. Groening, Periodic four-dimensional solution for transport of intense and coupled coasting beams through quadrupole channels, Phys. Rev. Accel. Beams **27**, 031602 (2024).

[10] D. Chernin, Evolution of rms beam envelopes in transport systems with linear $x - y$ coupling, Part. Accel. **24**, 24 (1988), https://cds.cern.ch/record/1053510/files/p29.pdf.

[11] C. Xiao, O. K. Kester, L. Groening, H. Leibrock, and M. Maier, Single-knob beamline for transverse emittance partitioning, Phys. Rev. ST Accel. Beams **16**, 044201 (2013).

[12] J. J. Barnard and B. Losic, Envelope modes of beams with angular momentum, in *Proceedings of the XXth International Linac Conference, Monterey, USA*, edited by A. W. Chao (Stanford Linear Accelerator Center, Stanford, USA, 2000).

[13] A. Burov, Circular modes for flat beams in the LHC, Phys. Rev. ST Accel. Beams **16**, 061002 (2013).

[14] Y.-L. Cheon, S.-H. Moon, M. Chung, and D.-O. Jeon, Effects of beam spinning on the fourth-order particle resonance of 3D bunched beams in high-intensity linear accelerator, Phys. Rev. Accel. Beams **25**, 064002 (2022).

[15] A. Hoover, N. J. Evans, and J. A. Holmes, Computation of the matched envelope of the Danilov distribution, Phys. Rev. Accel. Beams **24**, 044201 (2021).

[16] L. Groening, Considerations and findings on beam vorticity dynamics, arXiv:2401.13644v3.

[17] PTC Mathcad, https://www.ptc.com/en/engineering-math-software/mathcad.

[18] Y. K. Batygin, Particle-in-cell code Beampath for beam dynamics simulations in linear accelerators and beam lines, Nucl. Instrum. Methods Phys. Res., Sect. A **539**, 455 (2005).

[19] K. R. Crandall and D. P. Rusthoi, Documentation for Trace: An interactive beam-transport code, Internal Report No. LA-10235-M, Los Alamos National Laboratory, 1985, 10.2172/5937743.